VANADIUM IN PHYLLOSILICATES

by

Maxwell S. Drexler

A Thesis Submitted to the Faculty of the

DEPARTMENT OF MINING AND GEOLOGICAL ENGINEERING

In Partial Fulfillment of the Requirements

For the Degree of

MASTER OF SCIENCE

In the Graduate College

THE UNIVERSITY OF ARIZONA

2022

THE UNIVERSITY OF ARIZONA
GRADUATE COLLEGE

As members of the Master's Committee, we certify that we have read the thesis prepared by: Maxwell Drexler
titled: Vanadium in Phyllosilicates

and recommend that it be accepted as fulfilling the thesis requirement for the Master's Degree.

Isabel F. Barton
Isabel F. Barton Date: May 11, 2022

Jinhong Zhang Date: May 11, 2022

J. Brent Hiskey
J. Brent Hiskey Date: May 11, 2022

Final approval and acceptance of this thesis is contingent upon the candidate's submission of the final copies of the thesis to the Graduate College.

I hereby certify that I have read this thesis prepared under my direction and recommend that it be accepted as fulfilling the Master's requirement.

Isabel F. Barton
Isabel F. Barton Date: May 11, 2022
Thesis Committee Chair
Mining & Geological Engineering

Acknowledgements

We would like to acknowledge Drs. Thomas Zega, Jinhong Zhang, and Brent Hiskey at the University of Arizona for their comments on this work. Dr. Mark Barton provided use of the JEOL 6010LA SEM. Dr. Pierre-Marie Zanetta added invaluable expertise with the EELS technique and significant assistance with EELS data processing. Drs. Yao-Jen Chang and Zoe Zeszut of the Lunar and Planetary Laboratory provided expert assistance with the Hitachi HF-5000 Transmission Electron Microscope and FEI Helios SEM/FIB, respectively. Energy Fuels Inc., especially Dan Kapostasy, Timo Groves, and Logan Shumway provided technical assistance as well as access to samples and facilities. We thank the National Science Foundation (NSF) 20-54277 for funding this work.

Table of Contents

List of Figures

List of Tables

1.0 Abstract

Microscopic characterization of V-illites and V-chlorites investigated the role of V occurrence and V valence in the highly variable recovery of V from phyllosilicates in acid leaching. Scanning electron microscopy (SEM), transmission electron microscopy (TEM), and electron energy loss spectroscopy (EELS) were used to analyze V distribution on a nanometer scale and directly measure V redox state in silicate minerals, and the results were compared to the results of acid leaching experiments. EDS results show that V-illites are heterogenous in metal content. EELS measurements of V-illites identified a distinct nanometer scale V-oxide phase and showed that V in chlorites is more reduced vs. illites. V-chlorites have a more homogeneous V distribution and lacked a separate V-oxide phase. We suggest that the presence of nanoscale V-oxides in V-illites is responsible for variable, but sometimes higher V recovery of illite-rich ores vs. chlorite-rich ores. More generally, the presence of distinct microscopic phases within phyllosilicates is poorly understood yet may have significant economic impacts in mining, such as affecting metal extraction from phyllosilicate ores or gangue acid consumption.

2.0 Introduction

2.1 Modes of occurrence of metals in phyllosilicates

Metals have three distinct modes of occurrence in phyllosilicates. Metals may occur as non-phyllosilicates (e.g. native metals, metal oxides), within the phyllosilicate structure, forming inclusions at the submicron scale (Ahn et al., 1997; Baum, 1999; this work). A second type of occurrence is metal ions adsorbed onto the surfaces of clay minerals, which is responsible for the substantial preg-robbing capability of clays in copper heap leaching (Baum, 1999). The third mode of occurrence is metals bonded crystallographically in a mineral. Examples of minerals containing crystallographic metal include biotite, chlorite, and montmorillonite, which are

significant acid consumers in leaching (Baum, 1999; Jansen and Taylor, 2003, Chetty, 2018). Although the most abundant metals in most phyllosilicates are silicon, aluminum and iron, their crystal structures may accommodate significant lattice substitutions of Cu, Ni, V, Ti, and other metals with similar charge and ionic radius.

Understanding metal occurrence in phyllosilicates is important for a number of reasons. Phyllosilicates in general are responsible for metallurgical issues throughout the mineral processing value chain, particularly in leaching where their role in gangue acid consumption is connected to their extractable metal content. In addition, phyllosilicates can be important ore types, as is the case of vanadium-bearing phyllosilicates in the United States (Gao et al., 2021) and for laterite ores globally. However, not much is known about the nanoscale mechanisms of either metal extraction or gangue acid consumption in phyllosilicates. This study focuses on the occurrence and extraction of vanadium in phyllosilicate minerals as a case study with broader implications for both these phenomena.

2.2 Vanadium resources, production, and end use in the United States

Primary vanadium production in the United States mainly comes from Triassic or Jurassic sandstone-hosted uranium deposits in the Paradox Basin on the Colorado Plateau (Gao et al., 2021). In the Paradox Basin the principal vanadium ore minerals are generally a V-hydroxide phase, such as montroseite [(V,Fe)O(OH)], and/or a V phyllosilicate phase such as roscoelite, a V-bearing mica, idealized as $K(V,Al)_2(AlSi_3)O_{10}(OH)_2$, (Brigatti, 2003; Thorson, 2018). Other phyllosilicates, including smectite, illite, and chlorite, also host significant amounts of V in Jurassic rocks on the Colorado Plateau; duttonite is another common V-bearing hydroxide (Meunier, 1994; Radwany, 2021).

In 2020 the United States produced 170 metric tons of vanadium with an estimated value of $1.4 million, only 37% of 2019's V production (Polyak, 2021). This decrease is largely

attributed to ceasing byproduct production of vanadium from sandstones on the Colorado Plateau, due to a 53% decrease in vanadium price compared to 2019 (Polyak, 2021). Secondary vanadium production in the United States is primarily concentrated in Arkansas, Delaware, Ohio, Pennsylvania, and Texas, where processing of waste materials produces ferrovanadium, vanadium-bearing chemicals or alloys, vanadium metal, and vanadium pentoxide. From the period of 2016 – 2020, net import reliance as a percentage of apparent consumption in the United States varied from 94-100% (Polyak, 2021).

Vanadium's principal use is as a hardening agent in steel, where it improves toughness and wear resistance (Polyak, 2018). These properties are important in high-strength, low-alloy (< 0.15% V) steels. Catalysts are the greatest non-alloy use of vanadium. The metal is listed as a critical mineral by the U.S. Department of the Interior (Polyak, 2018). In addition, ongoing development of vanadium redox-flow batteries for large-scale energy storage represents a large potential increase in demand if technologies proceed to commercialization (Kear et al., 2011).

2.3 Extractive metallurgy of primary vanadium

Vanadium (V) exists in multiple oxidation states in natural systems. V^{3+}, V^{4+}, and V^{5+} may be present in over 300 minerals, forming at least nine ionic complexes in water at 25°C depending on the redox and pH conditions (Pourbaix, 1975; Gao et al., 2021). Traditionally, the first stage in vanadium-resource processing is salt roasting under oxidizing conditions in a rotary kiln or multiple-hearth roaster with a sodium salt, such as NaCl or $NaHCO_3$, while direct V-leaching is currently the preferred process. Roasting essentially converts the vanadium values into water-soluble polyvanadates, which can be leached by hot water leaching or alkali leaching from the calcine (Gupta, 1985). Direct sulfuric acid leaching is also applied to vanadium ores without prior processing, followed by recovery from the leach solution by ion exchange or solvent extraction (Baker and Sparling, 1981; Gupta, 1985). Though salt roasting was more

common in the past due to its higher V recovery, current US processes use direct leaching since both V and U can be extracted from the ores at lower cost (Baker and Sparling, 1981; Radwany and Barton, *in review*).

The complex mineralogy of V ores poses several challenges for extraction. The mineralogical complexity of vanadium ores, and their relatively low specific gravity, precludes processing by conventional gravity or flotation enrichment methods (Gupta, 1985). In hydrometallurgical operations, the solubility of vanadium oxides in acidic conditions can also be problematic. Tavakoli et al. (2014) found experimentally that V solubility in a sulfuric acid solution of pH 1.4 at 30°C is only 8.9 mM. Flowsheets for processing sandstone-hosted vanadium ores must also take into consideration that uranium is an important co-product (Baker and Sparling, 1981). Recovery for V is often below what is achieved in uranium processing, even at the same operation. For example, vanadium recovery by direct sulfuric acid leaching is around 65-71% at the Shaanxi Wuzhou Mining Co., Ltd. in China and around 75% at the White Mesa mill in Utah, USA (Baker and Sparling, 1981; Gao, 2021). Uranium recovery at the White Mesa mill is typically 95% and performed at the same grind size and leaching conditions as vanadium (Baker and Sparling, 1981). M. Radwany's geometallurgical study of U-V ores from the Colorado Plateau found that the main cause of suboptimal V recovery from the ores was low recovery from phyllosilicate minerals, which hosted on average 55% of the V contained in the ores. Though nearly complete recovery was obtained from V hydroxide minerals, extraction from phyllosilicates ranged from 0-35% across six samples in a sulfuric acid – sodium chlorate leaching system (Radwany, 2021). The variation did not appear to correlate with type of V-phyllosilicate or other discernible factors.

2.4 This study

This work investigates the leaching of vanadium-bearing phyllosilicate minerals as a case study of the mineralogical factors important to phyllosilicate leaching more broadly (Radwany, 2021). As detailed below, major questions include (1) the occurrence of V in phyllosilicates at the nanoscale, (2) the evolution of V phyllosilicates over the course of acid leaching, and (3) how leaching results are affected by V occurrence and crystal-chemical variations. For instance, one of the objectives of this study is to investigate whether there is a correlation between V's oxidation state and its extractability. It is conceivable that the proportions of V^{3+} and V^{4+} in minerals leads to significant recovery differences.

This question extends well beyond Paradox Basin V deposits. Improved fundamental understanding of silicate dissolution in general has important implications for predicting gangue-acid reactions and minimizing their negative effects in mining and metallurgical operations (Terry, 1983a). In copper heap leaching, acid consumption may represent up to 10-25% of the operating costs, much of which comes from unwanted leaching of phyllosilicates over long leaching times (Baum, 1999; Jansen and Taylor, 2003, Chetty, 2018). Data on the leaching of vanadium-bearing phyllosilicate minerals is applicable to our understanding of the dissolution of phyllosilicate gangue, and the related acid consumption, because these minerals likely behave similarly to their non-V-bearing analogs in extractive processes. The present work also has implications for recovery of V from other global resources, especially low-grade black shale aka 'stone coal' V deposits.

3.0 Literature Review

3.1 Geological Background

3.1.1 Paradox Basin, USA, geology

The provenance of the ores used in this study is the Pandora Mine, located in the La Sal District (Paradox Basin) of the Four Corners region of the United States, and the larger Colorado Plateau (Radwany, 2021). This district is a major domestic resource of vanadium and uranium ore, hosted in sandstones found in the Morrison Formation, which is of Jurassic age (Radwany, 2021). The Morrison formation also contains small copper deposits (Thorson, 2018). The formation of both the U-V deposits and the Cu deposits in the Morrison is tied to the complex history of paleofluid flow in the Morrison formation and larger Paradox Basin (reviewed in Thorson, 2018; Barton et al., 2018a,b).

Thorson (2018) reviews the geology of the Paradox Basin, and the following summary is mainly adapted from his description. The basin formed in the middle Pennsylvanian as a foreland basin due to thrusting on the Uncompaghre fault. For much of its history, the basin maintained shallow connections to the ocean, leading to repetitive cycles of desiccation and flooding as sea levels rose and fell. Desiccation periods caused deposition of an estimated 5,000 to 8,000 feet of salt and gypsum evaporites, with lesser amounts of dolomite, siltstone, and shales. In the Permian, the Paradox Basin was filled with clastic material from nearby uplifting, depositing conglomerates and sandstones to thicknesses varying with proximity to the uplift. During the Triassic and Jurassic, the basin was in a period of consistent continental conditions, recorded in the deposition of fluvial systems and eolian features, now largely red beds. The transgression of the Cretaceous Seaway sealed the Paradox Basin under thousands of feet of Mancos Shale. A geochemically complex series of fluids circulated throughout the basin, which is responsible for

the bleaching alteration of the sandstones in the region and the formation of economically important metal deposits (Thorson, 2018).

Paragenetic sequences of the U-V ores in the Paradox Basin on the Colorado Plateau provide some indication of the mechanisms that formed V deposits (Barton et al., 2018a). Based on textural relationships, asphalt or bitumen entered the porous sandstones and were then replaced by U minerals and V oxides (Barton et al, 2018a). Quartz overgrowths then captured and preserved some of these ore minerals during subsequent compaction and diagenesis (Barton et al., 2018a). Roscoelite and other V-phyllosilicates formed after this, utilizing some of the silica and metals that were liberated by continuing compaction and fluid circulation (Barton et al., 2018a). There is a large body of evidence supporting the hypothesis that U is transported in oxidizing fluids and precipitated by contacting reducing materials or fluids, and V probably behaves similarly, but variable U-V ratios in CO Plateau ores and the presence of V in bleached CO Plateau ores adds some ambiguity (Thorson, 2018). Still, a long history of previous work suggests that V is transported as V^{4+} in oxidizing fluids, then incorporated into ore minerals as V^{3+} by a reducing trap (Wanty et al., 1990; Thorson, 2018; Barton et al., 2018 (a)). This is essentially the reverse of hydrometallurgical processing of V, which requires oxidation of V to soluble V^{4+} or V^{5+} before leaching and subsequent separation.

V-Oxides and V-Hydroxides	V-silicates
Montroseite (V,Fe)OOH	***Roscoelite*** $K(V,Al,Mg)_2AlSi_3O_{10}(OH)_2$
Duttonite $(V,Fe)O(OH)_2$	***V-chlorite*** $(V,Fe,Mg,Al)_6(Si,Al)_4O_{10}(OH)_8$
	V-illite $K_{0.65}(V,Al)_2(Al,Si)_4O_{10}(OH)_2$

Table 1: Formulae of V minerals mentioned in section 3.1 (modified from Radwany, 2021).

3.2 Metallurgical Background

3.2.1 Vanadium in phyllosilicates

Common vanadium-bearing phyllosilicate minerals in the Paradox Basin are the V-bearing mica roscoelite, V-illite, and V-chlorite (Thorson, 2018; Radwany, 2021; Bos-Orent, 2021). The scanty literature on vanadium-bearing phyllosilicate minerals found in the United States generally concludes, through a combination of experiments and assumptions, that most V is contained crystallographically as lattice substitutions, mostly as V^{3+} (Foster, 1959; Meunier, 1994; Thorson, 2018; Radwany, 2021). Inclusions of V oxide or other phases have not been documented, and adsorbed V has been postulated but not observed (Peacor et al., 2000). The more detailed studies have indicated that there are complexities and significant unanswered questions about V siting and valence state (Foster, 1959; Wanty and Goldhaber, 1985; Meunier, 1994). The oxidation state and lattice siting of V in ore minerals is important to extractive metallurgy because it determines the bond strength and thus the extent of oxidation required to solubilize V. For example, V is thought to occur in roscoelite as V^{3+} bonded in the crystal's

octahedral site (Foster, 1959; Meunier, 1994; Peacor et al., 2000). However, Margaret D. Foster's (1959) chemical study, using acid digestion and titration, of mineralized clays from the Colorado Plateau found V to be structurally present in eight clay samples as V^{4+}, with one sample containing a mix of V^{3+} and V^{4+}. Analysis of the total charge of the clay minerals shows reasonable values only when formulas use V^{4+}, leading to the conclusion that V occurs in the clays in the V^{4+} state instead of the V^{3+} state (Foster, 1959). With increasing V content, both Al and Si contents decrease in the clays, indicating a coupled substitution. Leaching experiments indicated that V extraction-time curves follow closely the shape of Fe and Mg recovery curves (Foster, 1959). Because Fe and Mg are octahedrally coordinated in clays, Foster concluded that the V^{4+} present in these clay minerals is in the octahedral site. However, the correlation between increasing V and decreasing Si and Al is more consistent with V^{4+} in the tetrahedral site or with a combination of tetrahedral and octahedral occupancy, leaving the siting of V in phyllosilicates an open question.

Almost three decades after Foster's chemical study of mineralized clays from the Colorado Plateau, Wanty and Goldhaber (1984) returned to the idea of determining V and Fe oxidation states in oxides and silicates. The authors created a colorimetric method of determining V^{3+} without disturbing the original sample's V^{3+}/V^{tot} ratio, with the desire to apply the technique to understanding redox processes in ore genesis (Wanty and Goldhaber, 1984). After formulating and validating the procedure, the authors measured V^{3+}/V^{tot} ratios of two samples from Utah, one of a roscoelite and a second of a vanadium oxide mineral. Results from the roscoelite indicated a V^{3+}/V^{tot} ratio of 0.85. For the oxide mineral, the V^{3+}/V^{tot} ratio was found to be 0.37. Both Foster and Wanty et al.'s work show that phyllosilicates may contain a mix of V oxidation states (Foster, 1959; Wanty and Goldhaber, 1984). Despite these results, most other researchers

working on V-bearing phyllosilicates make the simplifying assumption that V is present as V^{3+} without utilizing an analytical technique sensitive to oxidation state (Meunier, 1994; Peacor et al., 2000; Radwany, 2021).

Scanning electron microscope (SEM) and electron microprobe (EMPA) analysis performed by J.D. Meunier on vanadium-bearing clay minerals in the Jurassic sandstones of the Colorado Plateau showed that the main V-clays are authigenic illite and chlorite (Meunier, 1994). By EMPA analysis, Meunier (1994) found that Al and V contents in both chlorite and illite are inversely coordinated, concluding that V replaces Al in the octahedral position. In the same study, Meunier also proposed a classification scheme that employs comparing V^{3+}/ the sum of the octahedral cations vs. the sum of the interlayer charges to distinguish V-illite and V-muscovite (Meunier, 1994).

Peacor et al. (2000) studied a V-bearing shale from a quarry in Velpen, Indiana with SEM and TEM to characterize V's occurrence in the rock. The authors found that V occurred in illite and an illite-smectite solid solution with an overall V content of 1.65 wt% V and composition of $K_{0.8}(Al_{2.8}Mg_{0.5}Fe_{0.4}V_{0.3})(Si_{7.2}Al_{0.8})O_{20}(OH)_4$. This formula was derived from EDS data and assumed an ideal dioctahedral structure with normalization to 12 tetrahedral plus octahedral cations (Peacor et al., 2000). Due to the relatively uniform distribution of V within the illite and illite-smectite, the group concluded that V did not substitute into the minerals after formation but rather during diagenesis (Peacor et al., 2000). Because TEM with EDS is not capable of directly measuring oxidation states, however, the study assumed that all V is present as V^{3+} in the octahedral site.

3.2.2 Acid dissolution of silicates

Several studies have addressed the acid dissolution of phyllosilicates in various contexts, including metallurgical. G. J. Ross (1969) studied the acid dissolution of chlorite samples in Si-

saturated 2N HCl and correlated leaching observations with the crystal-chemical siting of the metals. Unlike previous researchers, Ross found that the minerals released Mg, Fe, and Al at equal rates (Ross, 1969). This implied that octahedrally coordinated cations dissolve at the largely same rate as cations in tetrahedral coordination, despite bonding strength differences. Ross suggested, therefore, that the dissolution reaction appears to be diffusion controlled (Ross, 1969).

Other researchers concluded that octahedrally coordinated cations dissolve faster than tetrahedrally coordinated cations (Brindley and Youell, 1951; Osthaus, 1953; Delvaux, 1966). By analyzing the leaching of a magnesian chlorite by acid at constant temperature, Brindley and Youell (1951) found initially identical recovery vs. time for Mg, Fe, H_2O, and Al, but Al extraction proceeded much more slowly after about 47% recovery. The authors took this extraction to represent the limit of octahedral aluminum, agreeing closely with the mineral's ideal chemical formula in which half the Al is tetrahedral, and found by XRD that the mineral effectively becomes amorphous when octahedral Al is removed (Brindley and Youell, 1951). Similarly, Osthaus (1953) leached nontronite and montmorillonite samples in dilute HCl and plotted recovery-time curves of major cations. He found two distinct slopes of the recovery-time curves, indicating a change in reaction rate (Osthaus, 1953). He too concluded that the octahedral layer was first dissolving, followed by the tetrahedral layers at a much slower rate. It is noteworthy that one montmorillonite sample showed no substitution of Al for Si in the tetrahedral layer (Osthaus, 1953). Most researchers conclude that V is present in the octahedral site, which the workers above have shown is more amenable to dissolution, and therefore leaching (Foster, 1959; Meunier, 1994; Brandt et al., 2003; Thorson, 2018; Radwany, 2021).

Contrarily, if V is present in the tetrahedral site of a phyllosilicate mineral it would be significantly more difficult to extract.

In a three-part series of papers published in *Hydrometallurgy* in 1983, B. Terry discussed 'The Acid Decomposition of Silicate Minerals' and how it pertains to hydrometallurgists (Terry, 1983). Silicates may decompose in three ways: complete breakdown and dissolution of silicate, leading to formation of a silica gel by polymerization; partial decomposition of the structure leading to dissolution of cations and leaving a siliceous residue; or essentially no reaction at all. In hydrometallurgy, the partial decomposition of silicates is generally preferred because formation of silica gels can have serious consequences in the subsequent processing of the leach liquor. Silicates' reactivities in acids relate to their arrangement of silicon-oxygen tetrahedra (i.e., orthosilicates, sorosilicates, cyclosilicates, inosilicates, phyllosilicates, and tectosilicates Terry; 1983). He found that generally, the increasing silicate polymerization of this series correlates to a reduced susceptibility to dissolution in acids (Terry, 1983). This is consistent with the greater stability of felsic minerals in acid, as indicated by Bowen's reaction series and other geochemical fundamentals, as well as higher average bond strengths in highly polymerized minerals.

Oelkers (2001) developed a general kinetic description of multi-oxide silicate mineral and glass dissolution based on the results of a large body of experimental work performed on single and multioxide silicate minerals. In silicate dissolution, the precursor complexes are a series of metal-proton exchange reactions with partially liberated metals near the surface (Oelkers, 2001). The law of mass action can then be used to determine the relationship between rate-controlling precursor complex formation and aqueous solution composition and compared to experimental results. Oelkers (2001) developed a general chemical formula expressing the

relationship between the stochiometric number of metal atoms in a mineral normalized to the formation of the precursor complex, the metal's valence, the number of protons, and the formation of metal complexes.

In 2001, Bickmore et al. performed an in-situ atomic force microscope (AFM) study of the dissolution of two smectite minerals, hectorite and nontronite in acid solutions. The authors observed, as expected, that the crystallites dissolved inward from the edges, and the basal surfaces were unreactive during the timescale of the experiments. They explain this observation using periodic chain bond theory to predict the surface functional groups on the faces of the minerals. The periodic chain bond theory predicts that if a certain amount of surface relaxation occurs on specific crystal faces a stability difference becomes apparent in which crystal edges, but not the basal planes, are under bonded to connecting oxygen atoms (Bickmore et al., 2001). This implies that the rate limiting step of the dissolution process is the breaking of bonds to connecting oxygen atoms (Bickmore et al., 2001). Due to the phyllosilicates' layer structure, most of the surface area of these minerals is on the basal plane. From first principles considerations, it is unsurprising that dissolution occurs fastest along crystal edges.

Experiments on the effect of pH and temperature on the kinetics of montmorillonite dissolution showed that dissolution is initially incongruent but approached congruency at longer leaching times (Rozalen et al., 2009). The group performed experiments on montmorillonite samples at 50 and 70°C in flow-through reactors over a pH range of 1-13.5. Measuring the Al/Si ratio in solution at regular intervals during the experiments and comparing it to the stochiometric Al/Si ratio of smectite permitted the researchers to estimate the level of congruency in the dissolution (Rozalen et al., 2009). Generally, results indicated that montmorillonite dissolves incongruently initially while solutions progressively approach an Al/Si ratio of the mineral itself,

reaching congruent dissolution around 1000-2000 hrs of dissolution at 50°C and faster at higher temperatures. Comparison with experimental studies on other sheet silicates, including chlorite and illite, shows a similar relationship between dissolution rate and pH, suggesting that they too dissolve incongruently (Rozalen et al., 2009). It is likely that dissolution is incongruent until all alkalis and octahedrally coordinated cations, which are more weakly bonded than tetrahedra (Table 2), are dissolved, and thereafter dissolution proceeds congruently. It is likely that many V phyllosilicates also dissolve incongruently, with implications for the extraction of their metals.

3.3 Phyllosilicates in Extractive Hydrometallurgy

Chetty (2018) reviewed the practical importance of understanding silicate dissolution as it relates to the potential acid consumption of gangue, which is mainly composed of silicates (Chetty, 2018). Common minerals such as biotite, chlorite, epidote, pyroxene, and amphibole all exhibit significant solubility and consume acid. In the example of biotite, one mole of biotite dissolution will in theory consume 10 moles of protons if the reaction proceeds to completion, via equation (1).

$$K(Mg,Fe)_3(AlSi_3O_{10})(OH)_2 + 10H^+ = K^+ + Al^{3+} + 3H_4SiO_4 + 3(Fe,Mg)^{2+} \quad (1)$$

Snäll and Liljefors (2000) studied the leaching of major cations from common gangue minerals in varied strong acids and time intervals. They found high leachability (>80 wt.%) for most of the major cations in biotite and Mg-chlorite in 1M HCl in two hours, a significant finding for the acid consumption potential of these minerals in operations using acid curing and agglomeration (Snäll and Liljefors, 2000). An understanding of the gangue-acid reactions taking place in an operation, developed from characterizing pre- and post-reaction materials, would help determine the optimum addition of acid and water for effective curing and would yield better predictions of life-of-mine reagent costs (Chetty, 2018).

The dissolution of silicate gangue may also be problematic in maintaining acceptable heap permeability (Chetty, 2018). Precipitation of phases such as Al salts, jarosite, hydroxides, and other sulfates can lead to pore space clogging (Chetty, 2018) and can scavenge solubilized copper from the pregnant leach solution (PLS) in copper heap leaching (Baum, 1999). Given that the largest problem in copper and dump and heap leaching is that 70-80% of leach solutions flow over particle surfaces without penetrating in the rock matrix, it is important to understand, and limit, the precipitation of phases that decrease permeability and coat particles (Baum, 1999).

In addition, phyllosilicates may host variable but occasionally significant amounts of the target metal. A variety of phyllosilicate gangue in porphyry deposits, including biotite, chlorite, and illite have been shown to host anomalous copper concentration in different modes (Ilton and Verblen, 1993; Ahn, 1997). A study of samples from the Casa Grande porphyry copper deposit in Arizona using transmission electron microscopy (TEM) showed that biotite and chlorite from the chrysocolla zone of the deposit contain submicroscopic native copper inclusions, copper-rich expanded interlayers, and submicroscopic iron oxide inclusions (Ilton and Veblen, 1993). In other alteration areas of the deposit, biotite and chlorite contain only one mode of inclusion or none at all (Ilton and Veblen, 1993). Because copper anomalies appear correlated with supergene processes, the authors suggested that biotite and chlorite were enriched in copper during weathering, not by hydrothermal alteration, and suggest that phyllosilicates are a copper ‘sink’ in porphyry supergene environments much as they are on leach pads. Similarly, Ahn et al. (1993) found native copper inclusions in illite collected from the Picacho Mountains in Arizona and suggested that many sheet silicates may host similar inclusions. This study investigates whether such tiny inclusions of soluble V-oxides in insoluble V-phyllosilicates is a barrier to V recovery from selected Colorado Plateau, USA V ores.

V Redox State	V Coordination Number	Nominal Electrostatic Bond Strength
V^{3+}	6	0.50
V^{3+}	4	0.75
V^{4+}	6	0.33
V^{4+}	4	1.0

Table 2: Calculation of nominal V bond strengths based on the possible coordination and valence of V in phyllosilicates, following Pauling's rules.

4.0 Materials and Methods

4.1 Sample provenance

Samples for this project came from the ore head samples and leach residues of experimental work conducted by Radwany in 2020-2021. Radwany (2021) collected six ore samples on the Pandora Mine property of Energy Fuels Inc. Pandora is part of the La Sal mine complex on the Colorado Plateau in Utah and is mineralogically similar to other sandstone-hosted U-V ores in the region. The rocks were crushed, ground, and split, with some splits of each sample mounted in epoxy for mineralogical analysis and others designated for leach testing (Radwany, 2021).

4.2 Summary of previous characterization

Thin sections of three of the six samples were made for optical petrographic characterization. For each sample, a total of 56 elements were analyzed using ICP-OES/MS after four-acid digestion, with a LECO carbon combustion assay as well (Radwany, 2021). Semi-quantitative mineralogical information of the samples came from analysis by the Tescan TIMA3 field emission SEM analyzer at the Freeport-McMoRan Tucson Technology Center. For details of the analytical methods and results, see Radwany (2021).

Briefly, the samples are quartz sandstones with minor feldspar, lithic clasts, and coalified plant material, with a range in SiO_2 content from 57% to 81% (Bos-Orent, 2021; Radwany, 2021). Vanadium and uranium oxides are found as tiny grains partly or fully enclosed within quartz rims, and more commonly as larger interstitial fillings between grains. Much of the rock matrix is vanadium phyllosilicates (Radwany, 2021).

The focus of this study was on samples LS01 and LS04, selected because they represent two different types of V-phyllosilicate and two different levels of recovery. The V-phyllosilicate in LS01 was identified as an illite, compared to a V-chlorite in LS04. The chemical and mineralogical compositions of the overall samples are shown in Tables 3-4 below. The modal mineral abundance of LS01, determined by TESCAN TIMA showed that quartz makes up 89.1% of the rock, with vanadium phyllosilicates as 8.9% and vanadium hydroxides as 1.8% (Radwany, 2021).

Sample	**LS01**	**LS04**
Al (%)	0.65	1.97
C (%)	*b.d.*	*b.d.*
Ca (%)	0.06	0.09
Fe (%)	0.40	0.86
K (%)	0.31	0.34
Mg (%)	0.10	0.86
Na (%)	*b.d.*	0.08
P (%)	0.01	0.01
S (%)	0.13	0.13
Ti (%)	0.02	0.15
U (%)	0.05	0.19
V (%)	1.95	1.87
TotalACT (lb/t)	114	87
V/U	37.6	10.1

Table 3: Select whole-rock elemental assays of the six ore samples. b.d.=below detection limit. ACT= acid consumption (Radwany, 2021).

Phase	LS01	*LS01 σ*	LS04	*LS04 σ*
Quartz (%)	89.1	*0.56*	81.6	*0.46*
V-phyllosilicates (%)	8.9	*0.50*	14.8	*0.37*
V-hydroxide (%)	1.8	*0.04*	1.2	*0.08*
Uranium phases (%)	-	-	-	-
K-Feldspar (%)	-	-	1.1	*0.09*
All other phases (%)	0.19	*0.01*	1.23	*0.04*

Table 4: Modal mineralogy as determined by Tescan TIMA. Average and one standard deviation among the three replicates for each sample. Dash indicates the phase occurs as less than 1% by volume. Phases detected at less than 1% in all samples are not listed (Radwany, 2021).

4.3 Summary of previous leach test results

To investigate the geometallurgical behavior of the sampled vanadium ores, Radwany performed beaker leach tests at pH < 2 using 10 g/L sulfuric acid as a lixiviant and sodium chlorate as an oxidant, mimicking a current industrial process (Radwany, 2021). The oxidant kept the Eh between 600-800mV vs. Ag/AgCl. The experiments were done with 5 wt% solids at room temperature and agitated with a magnetic stir bar. Samples of the lixiviant solution were taken during the leach tests after 10, 20, 30, 60, 120, and 180 minutes of active leaching time using a syringe equipped with a 1 μm filter (Radwany, 2021). Results largely indicated that this time was sufficient to achieve ultimate recovery. Residues from the experiments were filtered, rinsed in deionized water, dried, and epoxy mounted for electron microprobe observation (Radwany, 2021). After a 1:150,000 dilution, the Arizona Laboratory for Emerging Contaminants (ALEC) at the University of Arizona analyzed solutions for V, Cr, Fe, Co, As, Se, and U (Radwany, 2021). Additional analyses for verification were performed at the Economic

Geology and Geometallurgy lab at the University of Arizona. The two labs used an Agilent 7700x and a ThermoFisher Element2 ICP-MS respectively.

For sample LS01, 53% of the vanadium leached in the acidic beaker test, compared to 14% for sample LS04 (Radwany, 2021). Electron microprobe analysis of the heads and tails showed that liberated vanadium hydroxides dissolved under the experimental conditions, but V-bearing phyllosilicates were present in the tails and showed variably poor V extraction. In the LS01 sample, about 36% of the V was extracted from the phyllosilicates, the highest of the samples tested. Extractions of V from other V-illites in samples LS02, LS03, and LS05 ranged from only 2-18%, for reasons that were not clear in the study (Radwany, 2021). Extraction of V from the V-chlorites in LS04 was negligible. Table 5 gives the EPMA compositions of the V-phyllosilicates in LS01 and LS04 before and after leaching from select grains, modified from Radwany (2021).

V-chlorite														
Sample #	**Material**	**Phase**	**Na**	**Mg**	**Al**	**Si**	**K**	**Ti**	**Ca**	**V**	**Fe**	**U**	**O** (calc)	**Total**
LS04	Head	V-chlorite	0	5.9	12	16.5	0.7	0	0	8.9	5	0	39.2	88.5
LS04	Head	V-chlorite	0	4.7	10.6	16.9	1.8	0.1	0.1	10.2	4.1	1.7	38.5	88.7
LS04	Head	V-chlorite	0.1	4	10	14.2	0.9	0.1	0.1	16.6	8	1.2	38.3	93.6
LS04	Head	V-chlorite	0.2	3.7	8	11.7	1.1	0.6	0	20.5	6.6	2.8	35.5	90.6
LS04	Tail	V-chlorite	0	6	11.9	15.9	0.8	0.2	0	7.8	4.6	0	38	85.5
V-illite														
Sample #	**Material**	**Phase**	**Na**	**Mg**	**Al**	**Si**	**K**	**Ti**	**Ca**	**V**	**Fe**	**U**	**O** (calc)	**Total**
LS01	Head	V-illite	0.2	0.7	9.8	17.7	6.2	0.1	0	17.7	1.3	0	39.4	93
LS01	Head	V-illite	0.1	1.5	11.2	20	5.7	0.1	0	11.6	1.4	0	40.9	92.6
LS01	Head	V-illite	0.1	0.6	9.1	18.5	6	0	0	16.9	1.5	0.1	39.2	92.3
LS01	Head	V-illite	0.5	0.6	8.5	17.1	5	0.1	0	20.2	1.8	0	38.7	92.5
LS01	Tail	V-illite	0	0.5	7.7	19	5.7	0	0	10.5	1	0	39.9	84.3
LS01	Tail	V-illite	0	0.5	9.1	20.3	6.3	0	0	11.4	0.8	0	39.7	88.1
LS01	Tail	V-illite	0.1	1.5	10.1	22.8	5.1	0.1	0.1	6.4	2.4	0	40.8	89.4

Table 5: Compositions of V-illite and V-Chlorite grains determined by EMPA. Table modified from Radwany (2021).

The refractoriness of V in the phyllosilicate minerals is surprising, given the solubility of V under aggressive leaching conditions and the hypothesized location of V as octahedrally coordinated V^{3+} in these minerals (Foster, 1959; Munier, 1994), which should correlate with a solubility comparable to Al^{3+} (Brindley and Youell, 1951; Osthaus, 1953; Baum, 1999; Snäll and Liljefors, 2000; Chetty, 2018). This study is a geometallurgical investigation of the causes behind the low and variable extractability of V from the phyllosilicates using electron microscopy, with implications for the dissolution of V and other metals from phyllosilicates.

4.4 Analytical Methods – This Study

4.4.1 Benchtop JEOL 6010LA Scanning Electron Microscope (SEM)

A benchtop JEOL 6010LA SEM served in the identification and selection of phyllosilicate grains appropriate for TEM analysis. The JEOL microscope was typically operated with a 20kV accelerating voltage and 10mm working distance. An electron backscatter detector (BSE) combined with EDS permitted the selection of grains in head and tails samples with Al, Si, K, and V contents, corresponding to V-phyllosilicates. With this information, appropriate grains for TEM analysis were rapidly and accurately found on the focused ion beam (FIB) SEM, used to prepare a TEM lamella.

4.4.2 Preparation of TEM samples

Transmission electron microscopy requires an electron-transparent sample, which for silicates typically translates to a thickness around 50 nanometers. In this study, grains were prepared for TEM work by two methods. One was by focused ion beam (FIB) SEM, with a FEI Helios dual-beam Nanolab 660 equipped with a Tomahawk Ion Column gallium-source beam. The electron beam was used to image the sample, while the ion beam was used for imaging, milling, and carbon and platinum depositions. Imaging on the electron beam used an accelerating voltage of 5 kV and 0.40nA current. To protect the sample lamellae from ion beam damage during ion milling, a carbon capping layer of thickness near 500nm was first deposited with the electron beam at a voltage of 2kV and current of 3.2nA. Then, the ion beam deposited a second carbon capping layer of 2-3 micron thickness under an accelerating voltage of 30kV and current of 0.32nA. With the lamella area of the sample capped and protected from beam damage, it was extracted by milling with the ion beam at a voltage around 30kV and current ranging from 2.5 - 9.3 nA, depending on the hardness of the material and thickness of the lamella. Lower currents were used to protect the sample from beam damage as its thickness approached what is required for extraction of the lamellae with the needle, about 500 nanometers. After extraction of the lamella with the needle, it was welded to a copper TEM grid with more Pt deposition and thinned

again with the ion beam to reach a thickness around 50 nanometers, or less if possible. Importantly, the last thinning steps used progressively decreasing currents and voltages to assure that the lamella is free of beam damage that could potentially cause structural and chemical changes to the sample. Final thinning passes were done with an accelerating voltage of 8kV and current from 25-40 pA.

Due to a series of maintenance problems with the FIB-SEM, some samples had to be prepared by dispersion. Dry ore samples were sprinkled onto a copper TEM grid with amorphous carbon film. Inverting the TEM grid then allows large or poorly adhered particles to fall off and be collected, leaving the smallest particles behind. Comminution of the ores for metallurgical testing produced enough micron-sized particles for successful TEM analysis. The TEM's EDS capabilities allowed for identification of V-phyllosilicates. Most particles were electron transparent in at least some areas.

4.4.3 Hitachi HF5000 transmission electron microscope (TEM) procedure

Transmission electron microscopy (TEM) was utilized to elucidate some aspects of the leaching behavior of V in phyllosilicates. The TEM techniques used include energy-dispersive x-ray spectroscopy (EDS), electron diffraction, and electron energy loss spectroscopy (EELS). EDS measurements provide semi-quantitative, spatially resolved chemical information similar to the EDS on the standard SEM. Electron diffraction measurements use electrons diffracted by the crystal lattices of a sample to provide lattice spacing information, analogous to X-ray diffraction techniques but at a smaller scale. The EELS technique measures the amount of energy lost by beam electrons due to the inelastic interactions they experience going through a sample, which reflect the valence state and coordination of sample atoms or ions.

TEM work was done using a 200 keV Hitachi HF-5000 aberration-correcting microscope. The HF5000 is equipped with a cold-field emission gun, a third-order spherical

aberration corrector, bright-field (BF) and dark-field (DF) scanning TEM detectors, and two spectrometers: (1) an Oxford Instruments X-Max 100 TLE EDS system including twin, 100-mm^2 silicon-drift detectors and (2) a Gatan GIF Quantum ER (model 965) electron energy-loss spectrometer (EELS). The Quantum ER is a Gatan Imaging Filter equipped with a CCD detector and dual EELS capabilities, allowing low-loss and high-loss spectra to be acquired simultaneously. An EELS entrance aperture of 2.5mm and dispersion of 0.25 eV/channel provided acceptable resolution and a good signal to noise ratio.

4.8 Electron energy loss spectra (EELS) processing procedure

There are three main components to an EELS spectrum: the zero loss peak, the low-loss region, and the high-loss, a.k.a. core-loss region (reviewed by Kociak et al., 2011). Figure 1 shows the core-loss region of the V-oxide standards The core-loss region contains a lot of information about the chemical structure of the sample. Onsets of edges in the core region are related to electronic structure, bonding, and valence (Kociak et al., 2011). To investigate the valence and coordination states of V in phyllosilicate minerals, and the leaching implications, both V oxide standards and experimental head and tail samples were measured by EELS on the Hitachi HF-5000. Standards of synthetic V_2O_3, V_2O_4, and V_2O_5 were measured first to determine the chemical shift of V-L_2 and V-L_3 peak edges with V oxidation state changes. (A V metal standard was also measured but was not used in analyzing the data, since the absence of oxygen bonding makes its EELS spectrum differ substantially from those of V oxides or V silicates.) Spectra were processed using the HyperSpy open-source Python library. Zero loss peaks were aligned with the HyperSpy function and background signal was removed. The intensities of each spectrum were normalized to the largest peak intensity to remove the influence of concentration from the spectra. The energy axis of each spectrum was calibrated to a carbon high-loss

measurement and the zero-loss peak to ensure that the energy loss axis of each EELS spectrum is accurate. HyperSpy's Fourier transform function removed noise from the EELS signals.

Because the silicates may have V of mixed oxidation states, it is necessary to relate EELS spectral features to oxidation state by developing an oxidation state vs. spectral feature calibration curve on known standards and then solving for unknown samples' oxidation states. For the transition metals, a 'white-line ratio,' which is a ratio of the integrals of the L_3 and L_2 peaks, is an accepted method for relating spectral changes to oxidation state, as is observing the rightward L_2 peak shift with increasing oxidation state, named the 'chemical shift' (Tan et al., 2014; Slick et al., 2019). Due primarily to spectral similarities of the V^{3+} and V^{4+} oxides using the 0.25mV dispersion on the Hitachi HF-5000, neither the 'white line ratio' or 'chemical shift' produced satisfying results in determining the oxidation state of the V-silicate samples. Measuring the maximum peak height of the L_3 peak, however, proved to be useful. EELS measurements of the max L_3 peak height showed that peak height increases significantly from V^{3+} oxide to V^{5+}, as shown in Figure 1.

Natural samples measured by EELS included select illite samples of LS01 and chlorite samples of LS04. Additionally, a roscoelite sample from Placerville, Colorado and a natural V-oxide ore mineral were analyzed to provide an additional check on the results. All V-silicate samples show maximum L_3 peak heights between V^{3+} and V^{4+}, a result that would be expected for natural systems and one in good accordance with the existing literature on V-silicates (Foster, 1959; Wanty and Goldhaber, 1984).

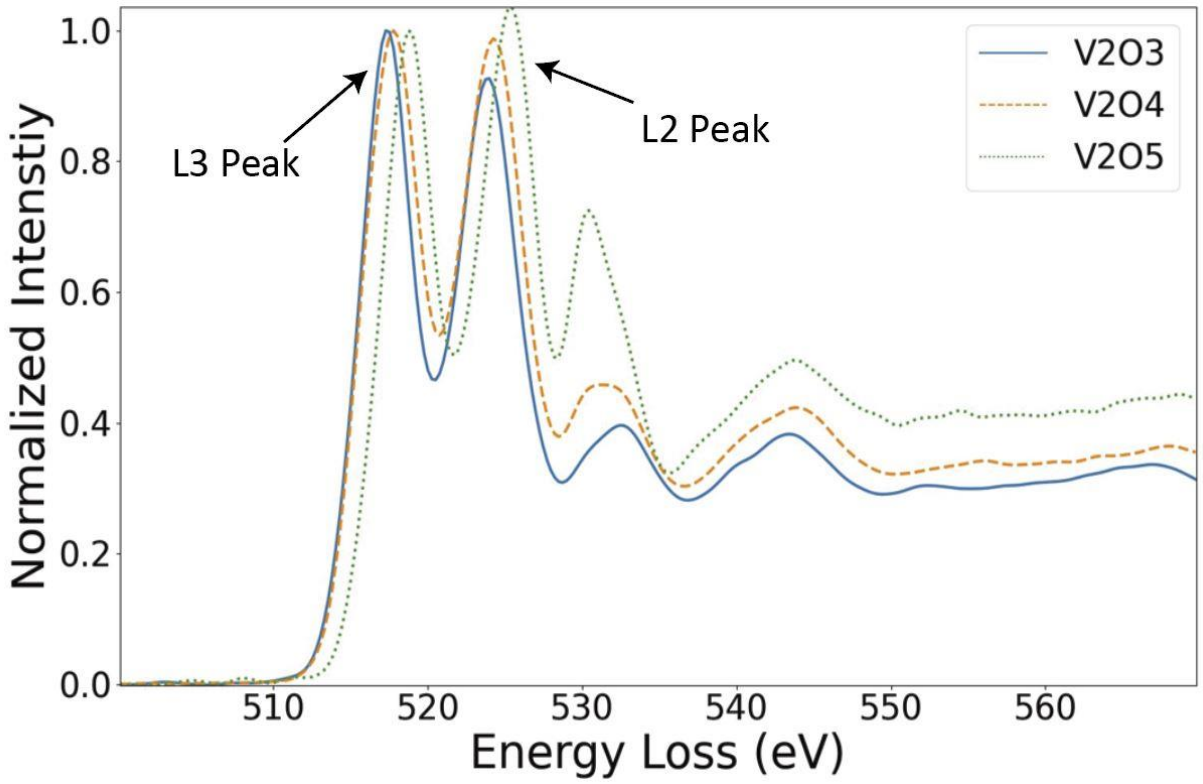

Figure 1: Electron energy loss spectra (EELS) for three vanadium standards, processed as described above. Spectra are normalized to the L_2 peak height.

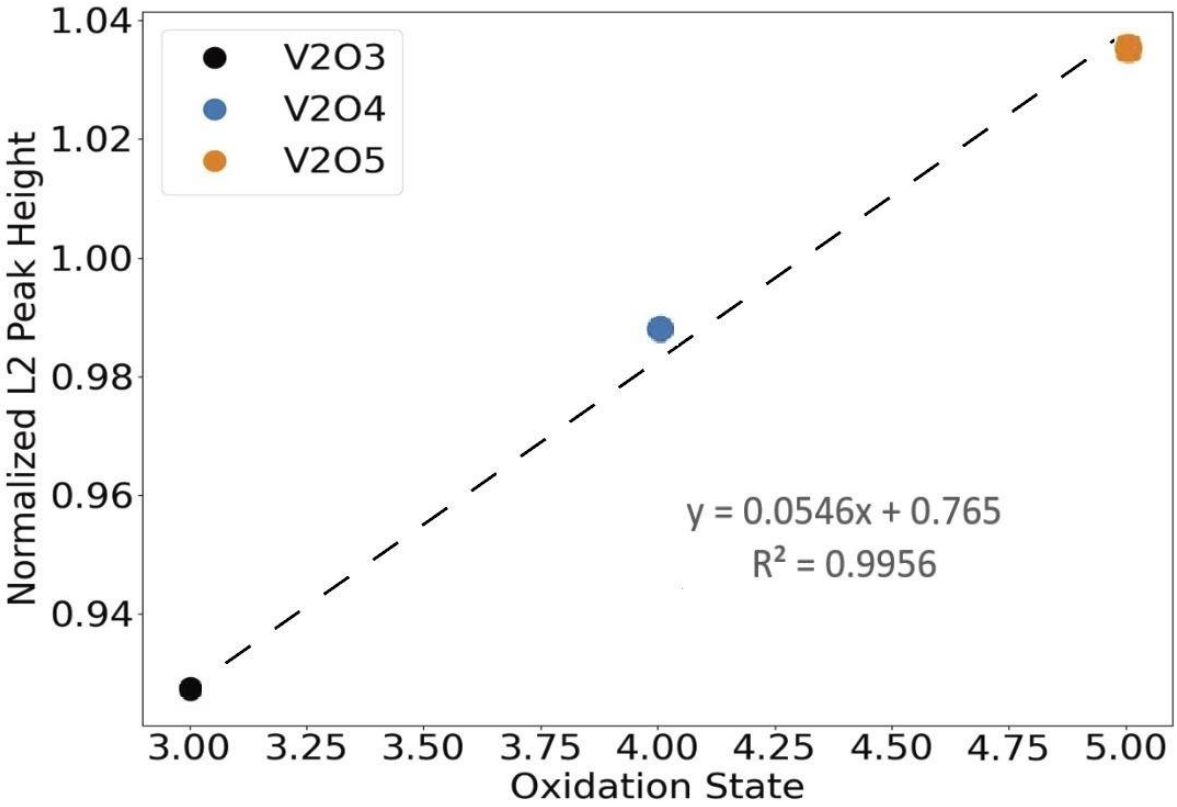

Figure 2: L2 Peak height vs. V oxidation state of V2O3, V2O4, and V2O5 standards after normalization of the individual spectra to their maximum L2 peak height.

5.0 Results

5.1 LS01 Illite Head Lamellae – Mineralogical Characterization by EDS and Imaging

A secondary electron (SE) imaging and EDS map of the V-illite lamella, Figure 3, shows textural and chemical heterogeneities in the illite. Perfect basal cleavage, characteristic of phyllosilicates, is evident in parts of the electron image. Electron diffraction results indicate a polycrystalline structure, as does textural evidence. Semi-quantitative energy-dispersive X-ray spectroscopy (EDS) results show the sample is approximately 29.6 wt % V_2O_3 (Table 6). EDS mapping reveals the heterogeneous distribution of the metal cations of particular interest to this study: Fe, V, Si, and Al. Generally, areas of higher V and Fe concentration occur in proximity to void spaces in the lamella (Figure 3).

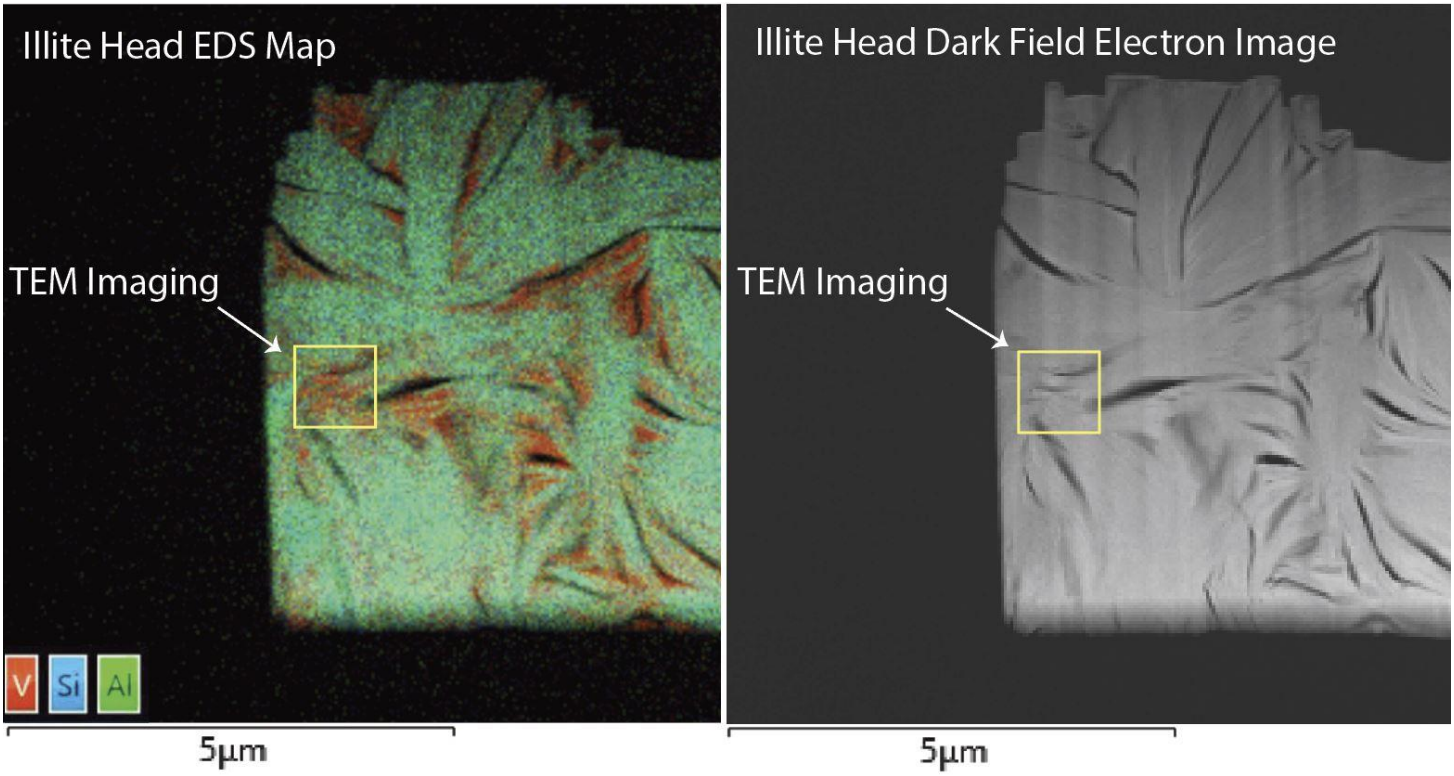

Figure 3: EDS mapping of the illite, showing high V and high Fe areas correlated to lower Al and Si concentrations. High-magnification TEM imaging of a high V area, shown in Figure 4, was done within the yellow box.

The significant heterogeneity in the distribution of metals throughout the illite head lamella, shown in Figure 3, raises the question of how the metal content is varying. High-V-Fe areas correlate inversely with Si and Al, suggesting a very high Fe and V content and low Si and Al within the illite structure, or the presence of a separate V-Fe phase in the red areas in Figure 3. One possibility is that there are nanoscale V-Fe oxides or hydroxides present as discrete edge phases within the V-illite, which would be consistent with the results of other work on Cu in illites (Ahn, 1997). A second possible causation of metal concentration heterogeneity is that metal cation ratios of are changing within the V-illite crystal lattice due to substitutions.

High resolution TEM imaging and EELS measurements were employed to investigate the crystallinity of the high-V areas in the yellow box in Figure 3, with the objective of determining whether they constitute a separate high-V mineral phase or a variation on the illite. The results are shown in Figure 4. In the center of the image, the c-axis of the mineral is oriented approximately perpendicular to the beam, making it possible to distinguish a layered lattice. Because the sample is polycrystalline with varied orientations it is impossible to orient the entire sample perpendicular to the electron beam. We did not clearly identify a separate V phase within the illite by TEM imaging. The layered structure observed could correspond to either a high-V illite or to a V oxide; V_2O_5 has a layered structure with perfect basal cleavage, similar to illite.

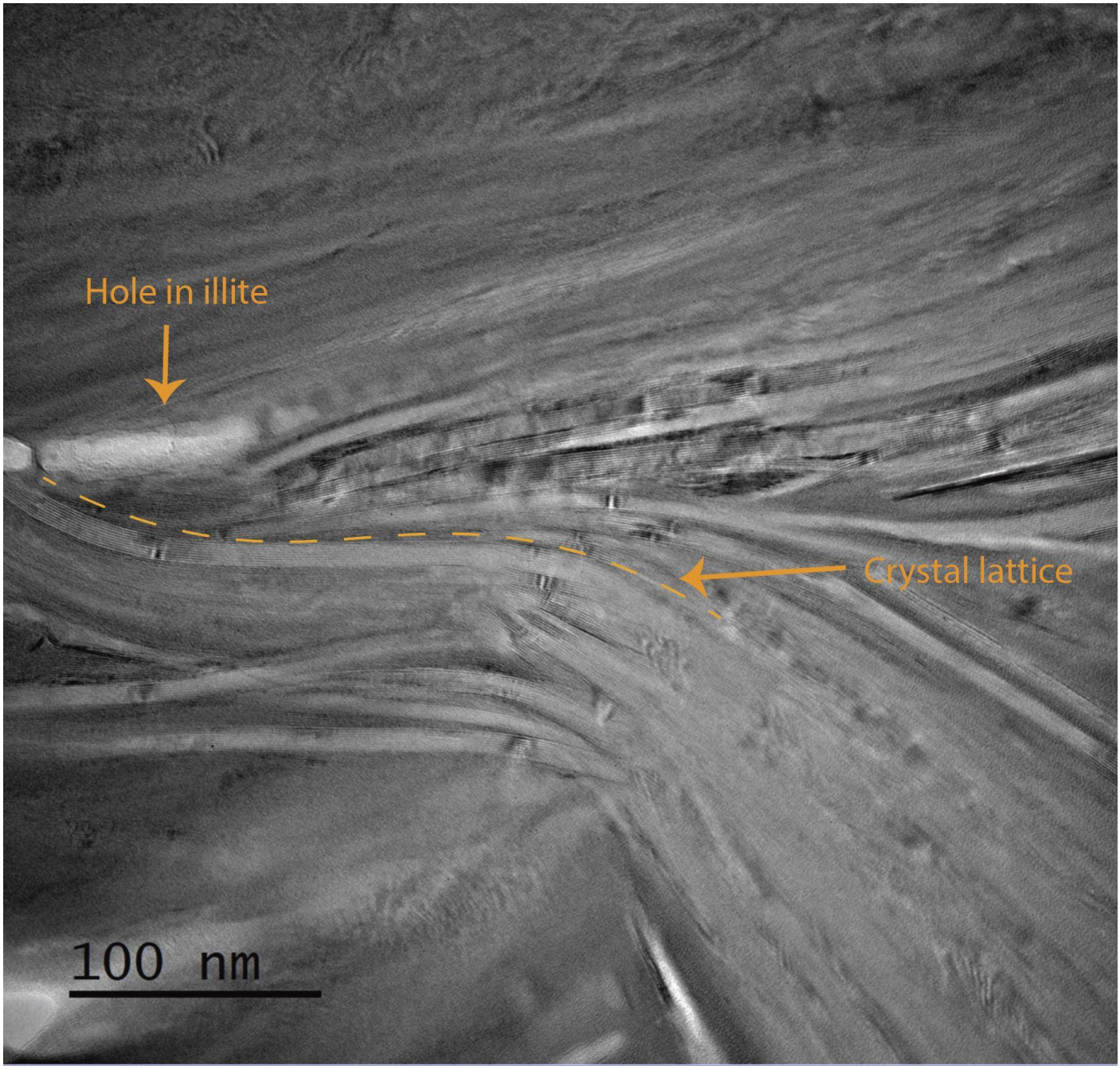

Figure 4: 120kX magnification bright-field image taken on the Hitachi HF5000 aberration-corrected TEM. In areas where the sample orientation is favorable, the phyllosilicate lattice can be seen running approximately E-W across the image.

Sample	Illite Head	Illite Tail 1	Illite Tail 2	Chlorite Head 1	Chlorite Head 2	Chlorite Head 3	Chlorite Tail 1	*Chlorite Tail 2	Chlorite Tail 3
Oxide (wt%)									
SiO_2	41.2	53.8	51.4	34.0	43.4	65.3	54.8	41.7	40.5
Al_2O_3	17.4	18.9	16.6	27.4	22.2	15.5	20.9	25.0	23.8
V_2O_3	29.6	16.1	20.7	14.1	17.1	6.7	9.4	10.8	14.0
K_2O	7.9	8.2	7.7	-	3.2	0.5	3.2	1.3	0.7
MgO	1.0	1.0	0.8	15.7	7.9	6.6	6.7	11.5	10.5
TiO_2	-	0.5	0.5	-	-	0.9	0.4	-	2.9
FeO	2.9	1.5	2.3	7.3	6.2	4.4	4.6	9.0	7.6
S	-	-	-	-	-	-	-	0.7	
Sigma (wt%)									
SiO_2	0.07	0.14	0.13	0.12	0.44	0.26	0.19	0.2	0.11
Al_2O_3	0.06	0.11	0.10	0.11	0.39	0.20	0.15	0.18	0.1
V_2O_3	0.07	0.11	0.11	0.04	0.36	0.15	0.12	0.15	0.09
K_2O	0.05	0.09	0.08	0.04	0.19	0.07	0.08	0.07	0.03
MgO	0.02	0.05	0.04	0.09	0.29	0.15	0.11	0.15	0.07
TiO_2	-	0.04	0.04	-	-	0.07	0.05	-	0.05
FeO	0.04	0.05	0.06	0.09	0.28	0.14	0.10	0.15	0.07
S	-	-	-	-	-	-	-	0.07	-

* Chlorite Tail 2 contains a pyrite grain

Table 6: EDS results for all samples analyzed on the Hitachi HF-5000 TEM expressed as oxide weight percentages.

5.2 Illite Tail – Mineralogical Characterization by EDS and Imaging

Electron imaging and EDS analysis of two illite tail (LS01) grains revealed one grain with less metal cation heterogeneity than the illite head sample (grain 1), and a second grain with significant metal cations heterogeneity, though somewhat less than the illite head. In illite tail grain 1, the metal content of V within the sample shows a ±5 wt% V variability, but EDS mapping does not show areas where V is the dominant cation at the expense of Si and Al, as is seen in parts of the head grain. Figures 5-6 show the EDS maps of illite tail grains, with Al, Fe, V, and Si chosen as the displayed elements.

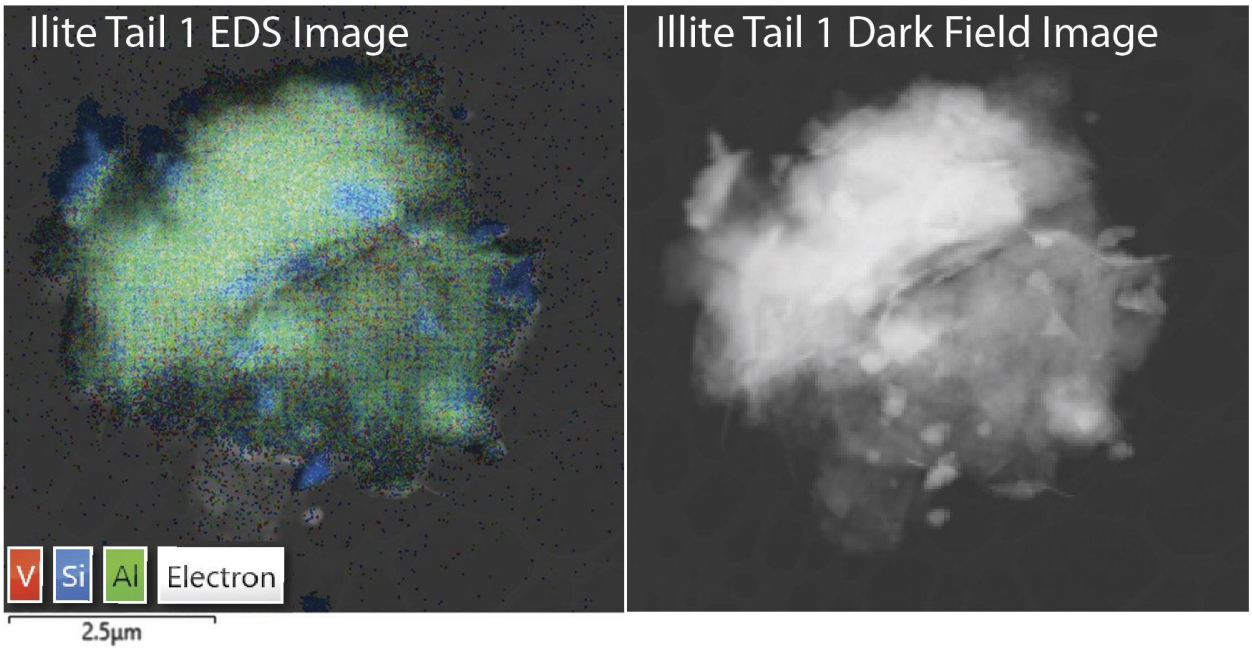

Figure 5: Layered EDS map of illite tail grain 1. This tail grain shows a more homogenous distribution of metal cations than tail grain 2 (Figure 6) and the illite head lamella (Figure 3).

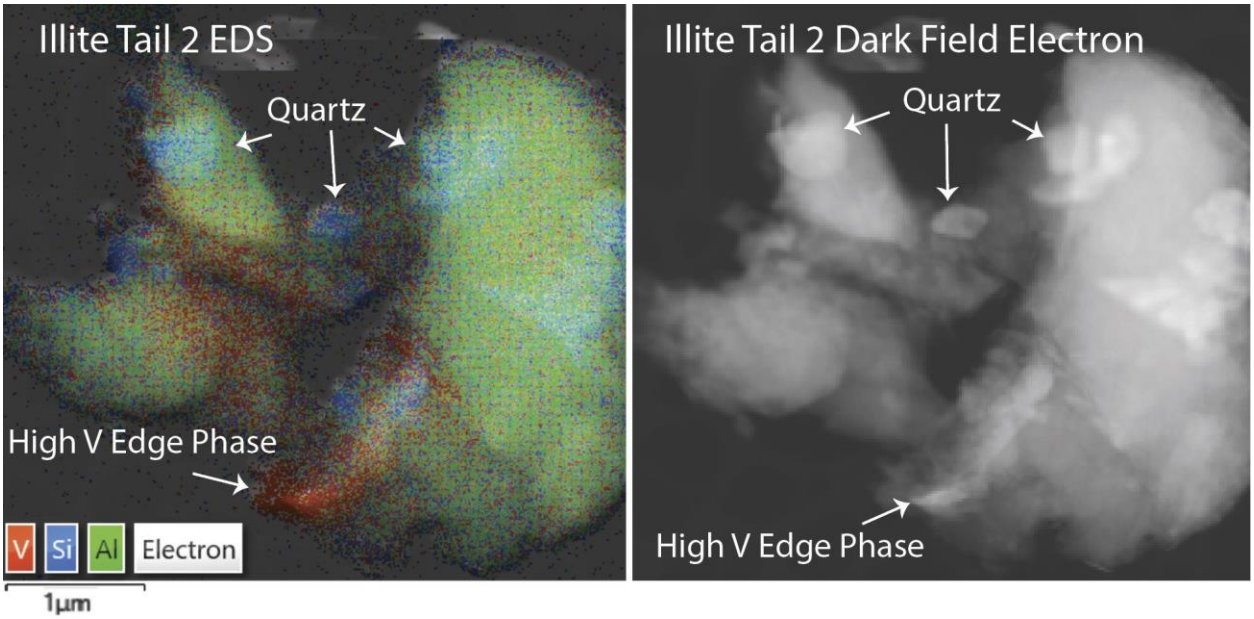

Figure 6: Layered EDS map of illite tail grain 2. Bright-green areas are significantly enriched in V and depleted in Si and Al, though less than the illite head.

Based on EDS results, both illite tail grains (outside of the high-V areas in tail grain 2) are depleted in V and Fe with respect to the illite head sample. The illite head sample FIB section

was approximately 29.6 wt% V_2O_3, whereas V content of the two tail grains ranges from 16.1-20.7 wt% V_2O_3 (Table 6). Overall, the tail grains retain much of their major metal cations, consistent with the electron microprobe results of Radwany (2021).

5.3 Chlorite Head (LS04) – Mineralogical Characterization by EDS and Imaging

Three phyllosilicate grains from the LS04 head sample were analyzed on the Hitachi HF-5000 by electron imaging and EDS. The compositions correspond to V-chlorite $(V,Fe,Mg,Al)_6(Si,Al)_4O_{10}(OH)_8$ with minor K (Radwany, 2021). Compared with the LS01 illite head, the LS04 chlorites are enriched in Fe and Mg, but contain les V (Table 6). The high SiO_2 in grain 3 appears to represent a V-chlorite grain underneath a quartz grain. Notably, the high-V areas identified in the LS01 V-illites (Fig. 3) were not found in any of the chlorite grains from the LS04 head sample (Figures 7-9).

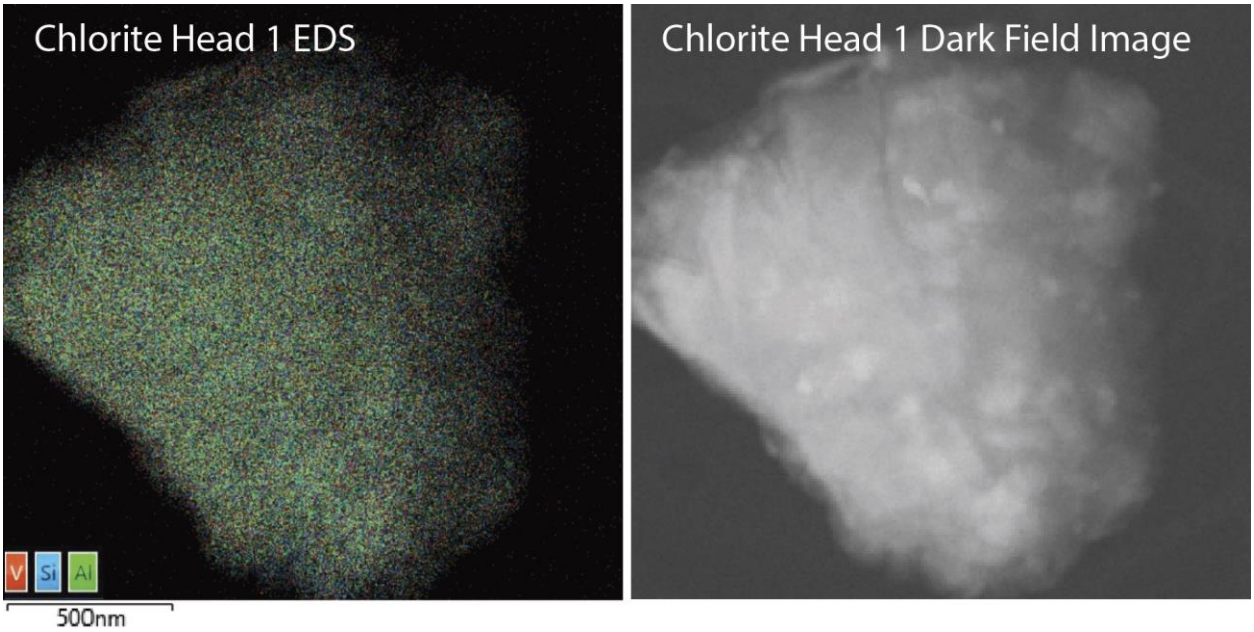

Figure 7: V-Si-Al EDS map of chlorite (LS04) head grain 1. Zones of anomalously high V concentration anti-correlated with Si and Al, aka V-edge phase, are notably absent in the chlorite.

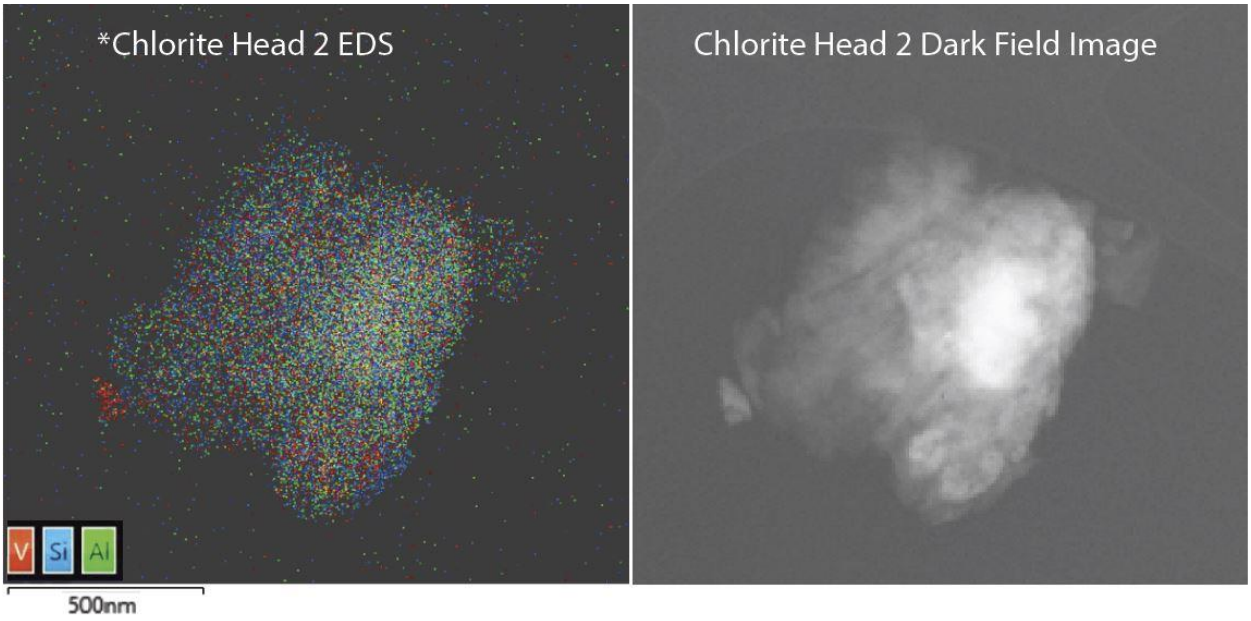

Figure 8: V-Si-Al EDS map of LS04 head grain 2. *Brightness and contrast of the EDS map were adjusted for legibility in in Oxford's AZtec software. Zones of anomalously high V concentration anti-correlated with Si and Al, aka V-edge phase, are notably absent in the chlorite.

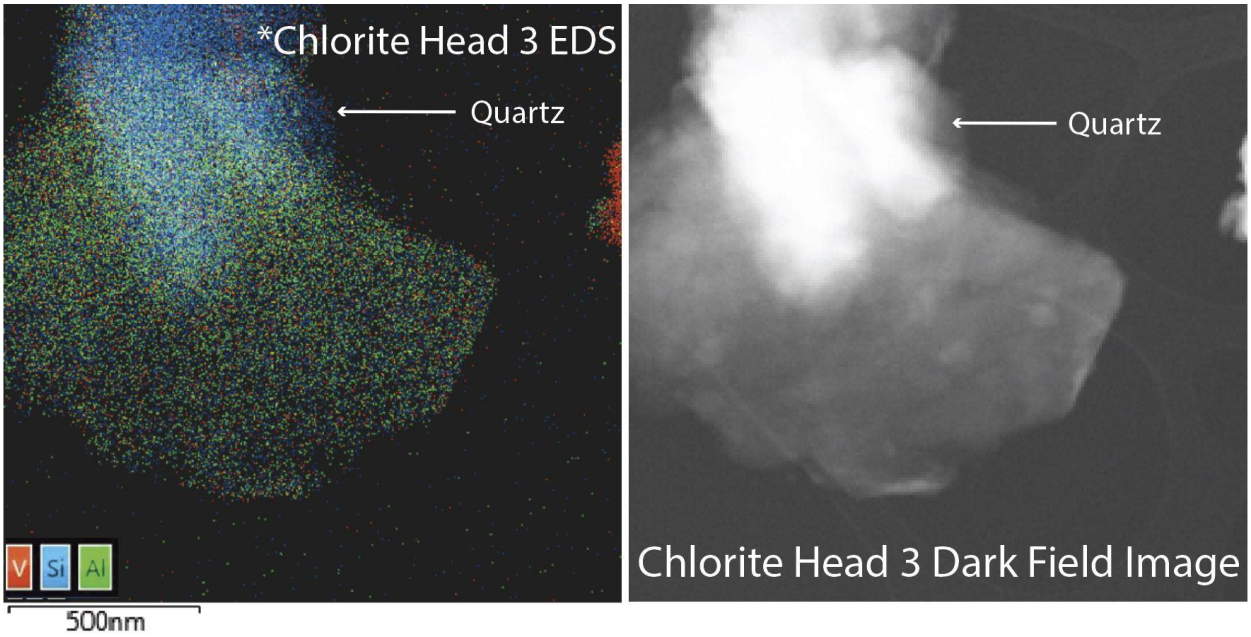

Figure 9: V-Si-Al EDS map of chlorite (LS04) head grain 3. *Brightness and contrast of the EDS map were adjusted for legibility in Oxford's AZtec software. The high-V edge phases anti-correlated with Si and Al, are notably absent. The bright region is interpreted as a quartz grain.

5.4 Chlorite Tail (LS04) - Mineralogical Characterization by EDS and Imaging

Three LS04 tail V-chlorite grains were analyzed by electron imaging and EDS. All three grains were polycrystalline, with the majority of the sample approximating a V-chlorite composition. Separate phases include quartz, pyrite, and a Ti-V oxide. Anomalously high-V zones of the sample appear only to correlate with Ti, suggesting discrete Ti-V oxides as the species Radwany (2021) observed these in both heads and tails, with textures suggesting detrital origin). V in the LS04 chlorites does not appear to create the high-V edge phases observed in the illite samples. EDS results show V_2O_3 contents in the tail samples are generally around 10 wt%, which is only slightly lower than LS04 head grains 1 and 2, which have grades over 15 wt% V_2O_3 as reported in Table 6.

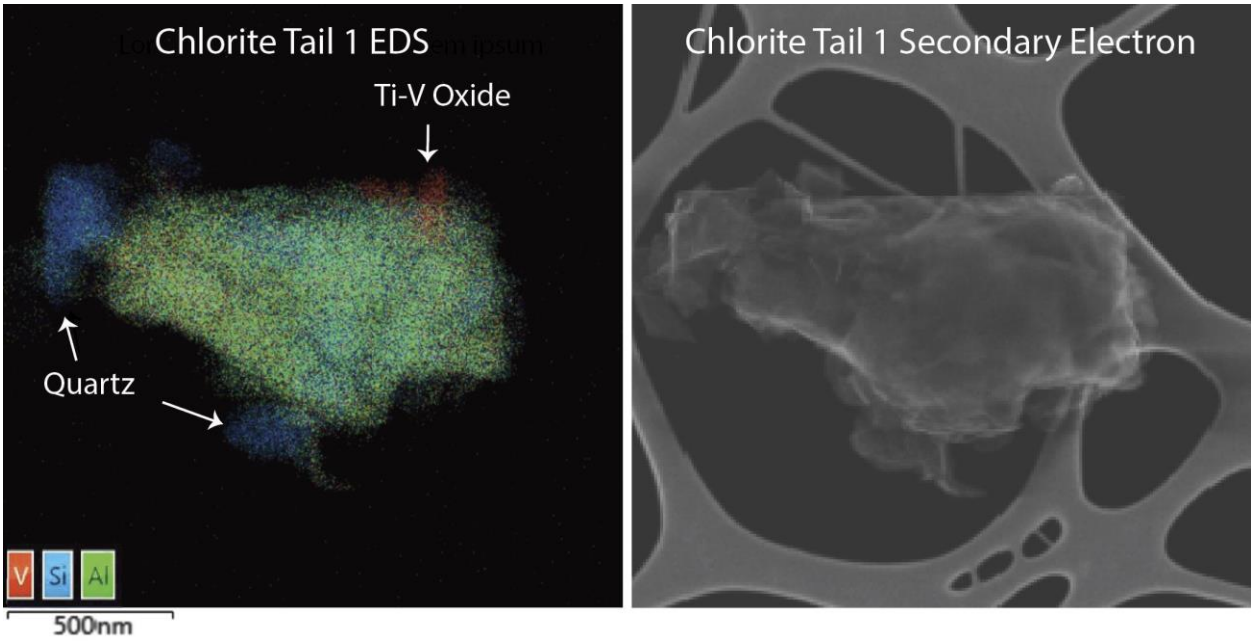

Figure 10: EDS V-Si-Al map of LS04 tail grain 1. Results indicate that the grain is polycrystalline, with two quartz grains (shown by high-Si and low-Al) and one Ti-V oxide grain agglomerated to a V-chlorite.

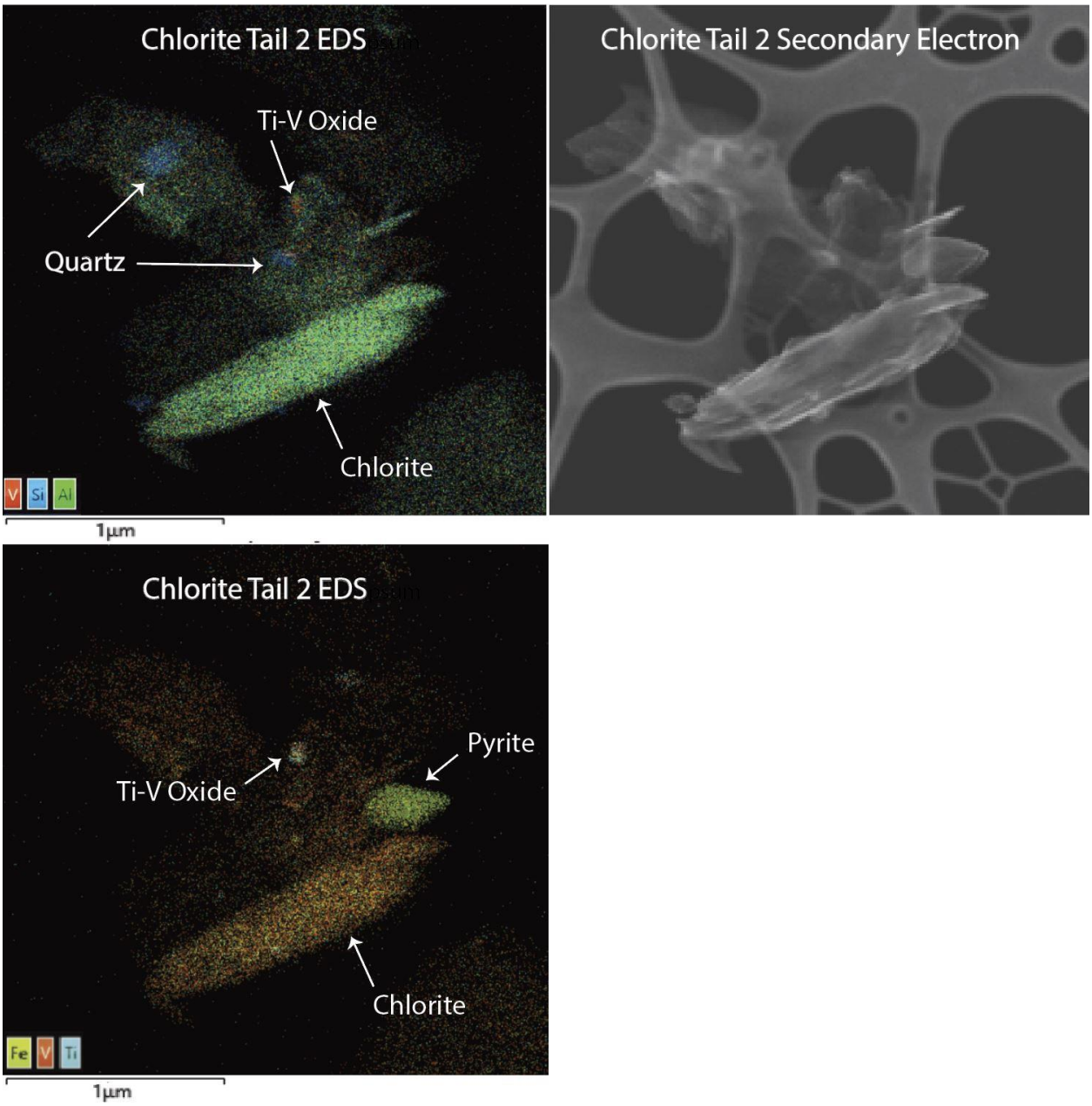

Figure 11: EDS V-Si-Al map of LS04 tail grain 2. Results indicate that the grain is polycrystalline, with two small quartz grains, one Ti-V oxide grain, and one pyrite grain agglomerated to a V-chlorite.

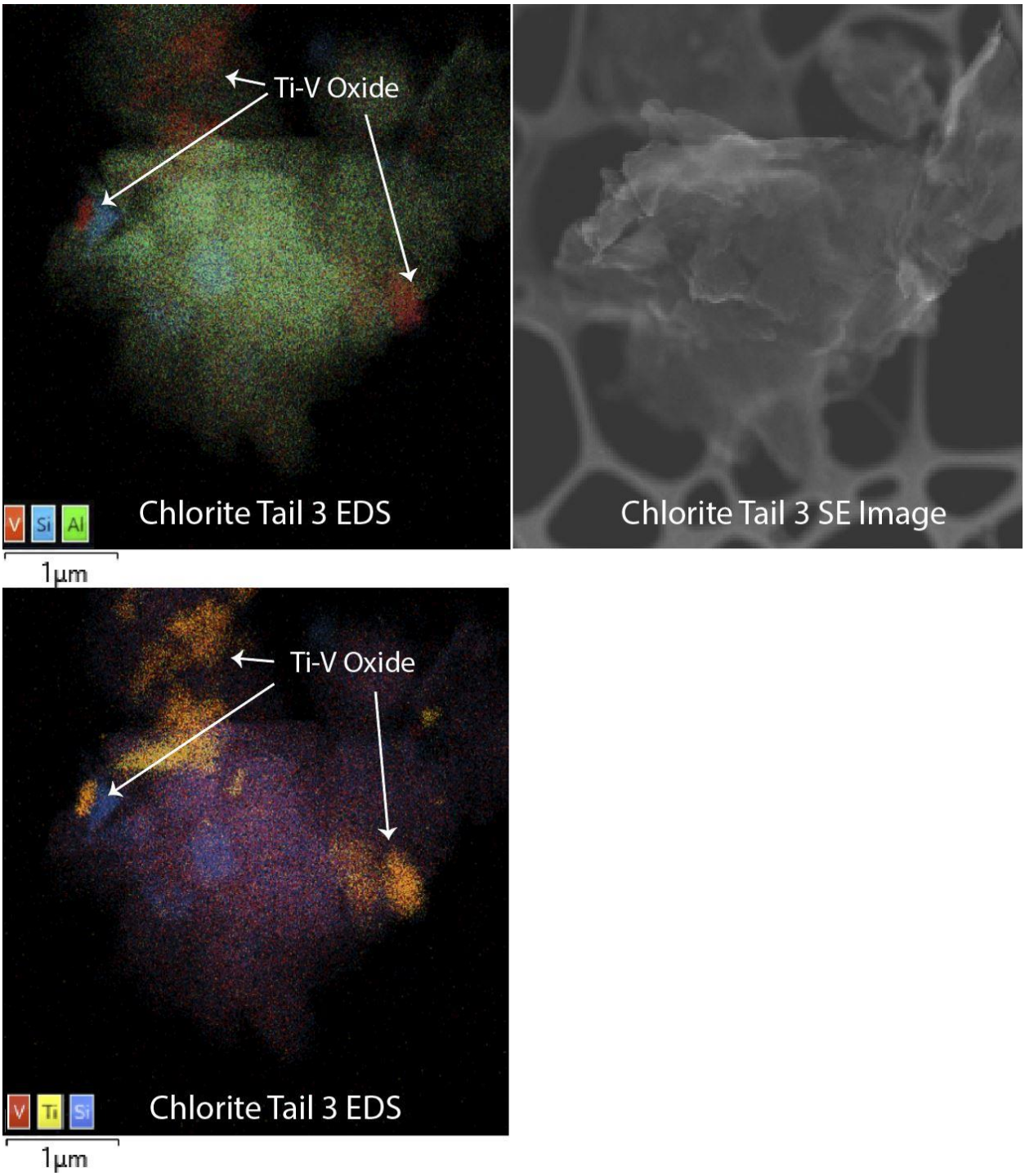

Figure 12: EDS V-Si-Al map chlorite (LS04) tail grain 3. See text for discussion.

5.5 Electron Energy Loss Spectroscopy (EELS) Results

EELS results are summarized in Table 7 and Figure 13, below. The V oxidation state of samples was determined by measuring the L_2 max peak height of the sample's near-edge energy loss structure and solving for the oxidation state using the developed standard curve, as described in section 4.8. All but one sample (the V oxide) plot as a mixture of V^{3+} and V^{4+}.

Several interesting trends are noticeable in the EELS results (Figure 13). Overall, chlorite samples plot as much more reduced compared to the illites. For the chlorites, the majority of contained V is present in the V^{3+} oxidation state. Illite samples are more oxidized, containing the majority of their V in the V^{4+} oxidation state. One natural V-Fe oxide mineral was measured, and its L_2 max peak height matches the VO_2 peak very closely, showing that V^{4+} oxides are present in the ore. The roscoelite sample from Placerville, CO plots at an intermediate composition between the chlorites and illites. Average oxidation states are shown in Table 7.

EELS spectra of the high-V areas present in the Illite 1 Tail sample are distinct from those of the V-silicates, indicating that the high-V areas are V-oxide, and therefore a separate V edge phase rather than high-V zones in illite. Figure 14 shows the spectra of the following samples: 'Illite Tail 1 High V Edge Phase', V_2O_5, V_2O_4 and the roscoelite sample. Interestingly, Figure 14 clearly displays the similarities in the O-K regions (near 530eV) of the spectra for the 'Illite Tail 1 High V Edge Phase' and V_2O_5 and V_2O_4 samples, whereas all the silicates show a high-intensity O-K region, like the roscoelite. The 'Illite Tail High V Edge phase 2' measurement shows an L_2 peak height greater than that of V_2O_4 and may therefore contain appreciable V^{5+}.

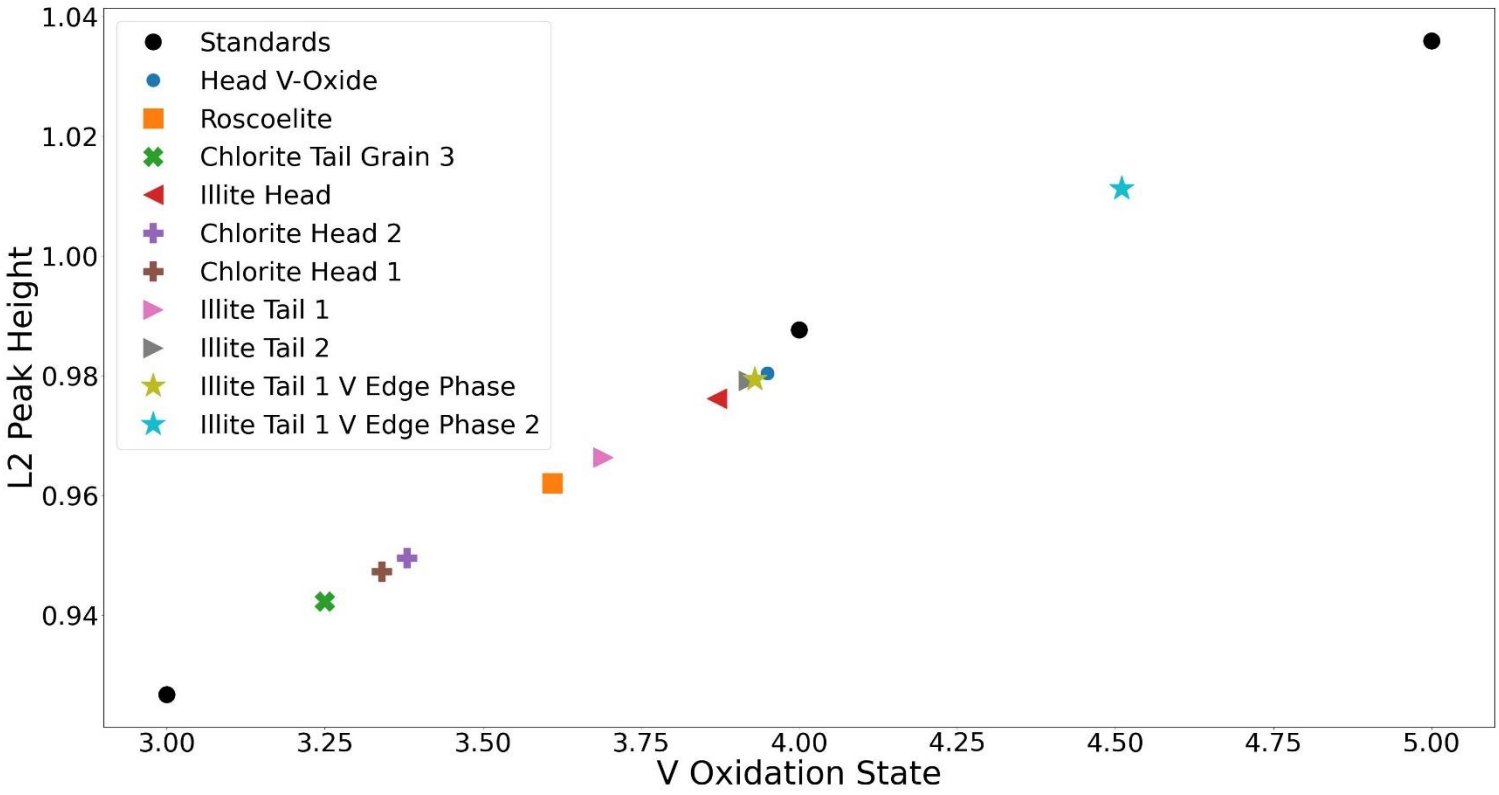

Figure 13: Plot of max L_2 peak height vs. oxidation state for known V valence standards and unknown V valence samples (see Methods section 4.8). Overall, chlorites plot as more reduced than the illite samples.

Sample	L_2 Peak Max Height	V Oxidation State	$\%V^{3+}$	$\%V^{4+}$	$\%V^{5+}$
***V_2O_3 (V^{3+})**	0.9267	3.0	100.0	-	-
***VO_2 (V^{4+})**	0.9876	4.0	-	100.0	-
***V_2O_5 (V^{5+})**	1.0359	5.0	-	-	100.0
Chlorite Tail Grain 3 (LS04)	0.9422	3.25	74.5	25.5	-
Chlorite Head 1 (LS04)	0.9473	3.34	65.1	34.9	-
Chlorite Head 2 (LS04)	0.9496	3.38	60.9	39.1	-
Roscoelite	0.9621	3.61	39.0	61.0	-
Illite Tail 1 (LS01)	0.9663	3.69	30.3	69.7	-
Illite Head 1 (LS01)	0.9761	3.87	12.4	87.6	-
Illite Tail 2 (LS01)	0.9792	3.92	6.7	93.3	-
Illite Tail 1 V Edge Phase	0.9794	3.93	6.3	93.7	-
Head V-Oxide (LS04)	0.9804	3.95	4.5	95.5	-
Illite Tail 1 V Edge Phase 2	1.0113	4.51	-	48.9	51.1

* V oxide standard

Table 7: V oxidation state results determined by EELS. Samples are arranged as reduced to oxidized from top to bottom.

Sample	L_2/L_3 Peak Height
V_2O_3 (V^{3+})	0.926
VO_2 (V^{4+})	0.987
V_2O_5 (V^{5+})	1.036
Roscoelite	0.962
Illite Head 1 (LS01)	0.976
Head V-Oxide (LS04)	0.980
Chlorite Tail (LS04)	0.942
Chlorite Head 2 (LS04)	0.952
Illite Tail High [V] 1	0.979
Chlorite Head 1 (LS04)	0.947
Illite Tail High [V] 2	1.011
Illite Tail 1 (LS01)	0.966
Illite Tail 2 (LS01)	0.979

Measurement Statistics	
Standard Deviation	0.028
Range	0.110
Mean	0.973
Chlorite Mean	0.947
Illite Mean	0.974
Illite Mean – Chlorite Mean	0.027

Table 8: Report of the normalized L_2 peak height for the dataset. The mean of the chlorites and illites are separated by about one standard deviation.

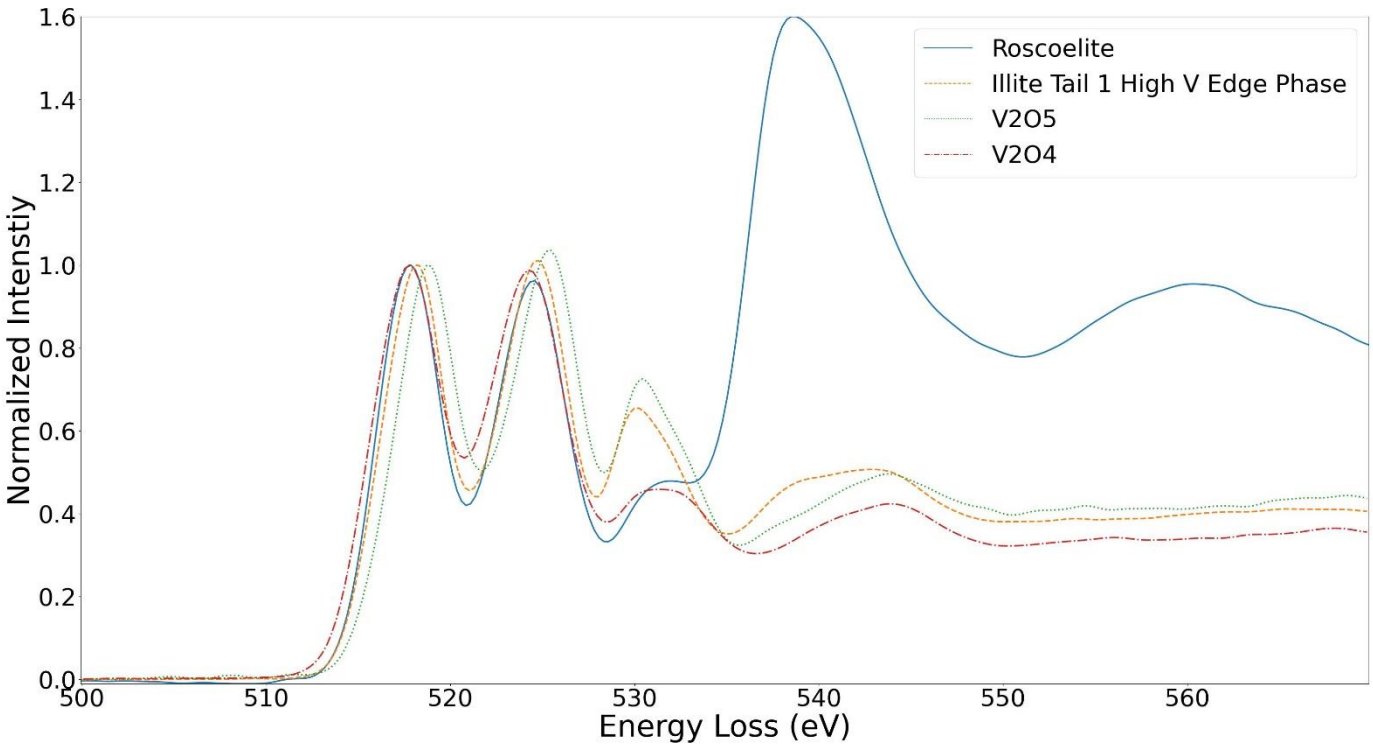

Figure 14: EELS results for the V_2O_4 oxide, V_2O_5 oxide, roscoelite, and the high-V edge phase of an illite sample, showing the similarity between the edge phase and the oxides.

6.0 Discussion

6.1. Evaluation of results

The discovery of a nanoscale high-V edge phase, which has different bonding and metallurgical behavior from the illite, is new information that helps explain why the extraction of V from phyllosilicates can be quite complex, for example with what look like the same V-illites yielding very different recoveries. The data from this study indicate that separate, nanoscopic V-oxide phases might provide the majority of recovery from the more leachable sample, and that V-phyllosilicates with low recoveries are those where these high-V edge phases are scarce or absent. Predicting recovery for ores based on mineralogy therefore requires a good, complete understanding of mineralogy, including at a very small scale. However, the oxidation state of the

V does not appear to correlate with V recovery. Phyllosilicates have complex and variable metallurgical properties, as exemplified by this study, making detailed understanding a prerequisite to predicting their process behaviors.

6.2. V oxidation states –comparison with previous work

The EELS results for V valence determination largely agree with previous researchers' determinations that V oxides and silicates in practice contain a mix of V^{3+} and V^{4+} (silicates) and V^{4+} and V^{5+} (oxides) concentrations; the new data also extend the range of possible V^{4+} concentration (Foster, 1959; Wanty and Goldhaber, 1984). The eight clay samples that Foster (1959) analyzed ranged from 0-2.4 wt.% V^{5+}, 0-16.1 wt.% V^{4+}, and 0-1.4 wt.% V^{5+}. Wanty and Goldhaber (1984) reported the V valence results of a roscoelite sample from Placerville, Colorado. They found that 85% of the V was V^{3+} while we measured 39% V^{3+} by EELS in another roscoelite sample from the same locality. Wanty and Goldhaber (1984) also found only 37% of V as V^{3+} and the remainder as V^{4+} in a V-oxide sample from Hanksville, UT. Our V-oxide mineral result was about 5% V^{3+} and 95% V^{4+}. Wanty and Goldhaber's (1984) method relies on determination of V^{3+}/V^{tot}, and thus must assume the V^{tot} valence state, so our results are not directly comparable.

The methods employed by Foster and Wanty and Goldhaber (1959; 1984) computed a V valence state averaged over the entire sample, digested and analyzed. EELS results, however, are of a much higher resolution and therefore sensitive to the area of the grain chosen for analysis, without the bulk averaging of the colorimetric or titration methods. In addition, EELS analyses are usually done near the edges of particles where the sample is thinnest and electron-transparent. This opens up the possibility that the EELS measurements on the tail samples in this study were affected by leaching, which most strongly alters a mineral near the edges of the grain.

Natural sample variation may also account for the extended range of the V oxidation states determined by EELS, because the literature contains only a small dataset.

6.3. Implications for leaching (leaching V, then acid consumption)

6.3.1 Interpretation of V leaching results

Radwany (2021) reported higher V leaching recoveries from some but not all of the illites (~30% V recovery) and low recoveries from other illites and the chlorite. This conclusion was based on head and tail EMPA measurements, which average composition over a scale much larger than the TEM. The disparate leaching results may be explained by the fact that some of the illites contain high-V edge phases, and the chlorites do not. The EELS spectra of the high-V edge (Figure 14) suggest the edge phases are V-oxides, which are extremely soluble; being located near the edges of grains, they are also less likely to be locked by insoluble V-phyllosilicates. The correlation between higher V recovery from the illites and the presence of a separate V-oxide in these samples, offers an explanation for the improved illite recovery reported by Radwany (2021). The role of oxidation state is ambiguous. EELS results show that V in chlorites is more reduced than V in oxides, which in theory should mean that V in chlorites is more sensitive to oxidation. However, comparisons of TEM-EDS from heads and tails indicate that similar amounts of crystallographic V (i.e. non-edge-phases) was extracted from both illites and chlorites, making it difficult to conclusively determine if recoverability differences correlate at all with V valence variability.

6.3.2 Implications for other V deposits

V-bearing phyllosilicates are a significant world V resource, occurring in some sandstone-hosted vanadium (SSV) deposits and in black shales (Kelley et al., 2017). The United States is currently the main producer of V from SSV deposits, but very import reliant for vanadium (Kelley et al., 2017). In China, 87% of domestic vanadium reserves are contained in

black shale deposits, often referred to as ‘stone coal’ (Zhang et al., 2011). Ore minerals in these deposits are almost entirely V-phyllosilicates. A review paper on Chinese black shale deposits characterizes the V as most prevalent in the lattice of phyllosilicates, with minor amounts in organic compounds and as adsorbed species on clays, and rarely as another V-phase (Zhang et al., 2011). This paper, however, opens the possibility that significant amounts of V contained in black-shale phyllosilicates may in fact be a separate nanoscale phase.

A large number of papers have been recently published on the extractive metallurgy of the black shale deposits (Li et al., 2009; Zhang et al., 2011; Zheng et al., 2019). The studies usually identify the V-bearing silicate as ‘muscovite,’ which is the mineral roscoelite or a muscovite with significant V grade (Li et al., 2009; Zheng et al., 2019). Unfortunately, many of the metallurgical studies on the extraction of V from stone coal do not include characterization detailed enough to resolve the provenance of the recovered V (Li et al., 2009; Zheng et al., 2019). In the case of Li et al. (2009), V speciation was determined by diagnostic leaching, which has been shown to be an unreliable indicator of mineralogy (Baum, 1999). The authors also reported nearly equal components of V^{3+}, V^{4+}, and V^{5+}, but it is unclear how this valence state determination was made (Li et al., 2009).

Zheng et al. (2019a) attempted to model their V extraction results from black shale. They found that HF acid enhances V leaching by breaking down the octahedral layers of micas. In their experimental validation, they report higher recoveries of V than Mg, and Al, all of which are modelled under octahedral coordination. However, our results show that the characterization of their material may be inaccurate and therefore lead to incorrect conclusions. Zheng et al.’s (2019b) characterization consisted of a powder XRD analysis, identifying the most prominent peaks as quartz, muscovite, pyrite, and calcite, and composition by ICP-OES. SEM-EDS

indicates that the phyllosilicate mineral they studied contains 17.78 wt% Mg and only 0.65 wt % K (Zheng et al., 2019a,b). This sample contains too little K, and too much Mg, to be a muscovite, and may in fact be a clinochlore, based on chemistry alone. This invalidates most of their modeling, which was based on the assumption of a mica-type T-O-T structure. Clinochlore is a T-O structure, and thus an inappropriate sample to use for verifying the results of acid dissolution of a T-O-T phyllosilicate. Additionally, Zheng et al. assumed that the V in the mica is entirely V^{3+} within a phyllosilicate. The present results show that V phyllosilicate mineralogy and extractive metallurgy is complex and that V valence and speciation vary greatly in V-phyllosilicate ores.

Zeng et al. (2019 a,b) are not in agreement with the experimental literature on silicate dissolution when they conclude that the tetrahedral site of a T-O-T silicate must first be dissolved to liberate metals in the octahedral site and model accordingly. A large body of experimental work indicates that octahedrally coordinated metals dissolve before tetrahedrally coordinate metals, and that acid attack on the edges of the phyllosilicate sheets also occurs (Brindley and Youell, 1951; Osthaus, 1953; Ross, 1969; Kalinowski and Schweda, 1996). Consideration of the crystal chemistry of silicates generally shows that tetrahedral complexes are much more resistant to dissolution than octahedral structures (Terry, 1983).

This study reinforces the understanding of Radwany (2021) that phyllosilicate mineralogy is important to predicting leachability. Those results showed that V ores typically contain multiple V phyllosilicates, and that identifying the minerals chemically requires significant effort. The present study corroborates this and extends it to the nanoscale, where the ore mineralogy is also shown to influence extractability. If a V silicate ore contains most of the V as chlorite it is probably impossible to economically process, whereas a V-illite with a V-oxide

edge phase might yield higher leaching recovery. The presence of a more soluble, second metal phase on the edges of grains at the nanoscopic scale may drastically alter the economics of metal extraction from a phyllosilicate ore.

6.3.3 Implications for other commodities

The results of this study have implications for more than vanadium mining. Phyllosilicate gangue minerals are problematic long-term acid consumers in the processing of other commodities, like copper (Baum, 1999; Chetty, 2018). In this case, it is typically undesirable to leach metals from the phyllosilicate minerals because the reactions consume acid. Gangue phyllosilicates dissolve incongruently in acid leaching, and the acid-consuming reactions occur over a long term and may not be apparent in typical metallurgical testing (Terry, 1983; Baum, 1999; Chetty, 2018). Current practice in predicting acid consumption is to record the abundance of phyllosilicate gangue and assign each mineral some acid consumption value or ratio of mols acid consumed to mols mineral present (Baum, 1999). As this study shows, this approach (though useful) is a significant oversimplification. Just as small-scale mineralogical variation can affect metal recovery, it may also apply to metals exchanged for acid in more typical phyllosilicate gangue as well. For instance, the acid consumption of a biotite or chlorite might vary depending on whether it contains Fe as crystallographic, octahedrally coordinated Fe or as nanoscale Fe oxide grains. The same mineralogical complexities that make V recovery complicated are probably applicable to gangue acid consumption.

6.4 Future work

This study has shed light on how nanoscale variations in V valence and occurrence correlate with metallurgical extraction, but outstanding questions remain. Although our EELS results show that V phyllosilicates are a mix of V^{3+} and V^{4+}, it remains unclear if the V^{4+} is in the

tetrahedral site or in the octahedral site, which is important for understanding bond strength and leachability. Development of V-silicate standards for EELS measurements might be a method to resolve the V coordination question. The prevalence of nanoscale V-oxides in illites, and of nanoscale native metal or oxide phases within phyllosilicates in general, is not well-understood. The small number of samples examined in this study adds to the existing work but does not offer a basis for estimating how rare or common it is for phyllosilicates to contain metals as nanoscopic oxides compared to crystallographic ions. It also remains to be seen whether optimizing extraction plans to target the nanoscale phase, rather than the bulk refractory phyllosilicate, improves recoveries from phyllosilicate ores and/or raises gangue acid consumption in other operations. Our understanding of leach feed materials would benefit greatly from a combination of detailed characterization combined with metallurgical testing.

7.0 Conclusion

Metals in phyllosilicates may occur as adsorbed ions, as ions in the crystallographic lattice, or as nanoscopic but discrete grains of metals or metal oxides. In this case study, the occurrence and valence of V in phyllosilicate ores was examined and correlated with leachability. EDS analyses of a V-illite show anomalous areas of high-V content with lower Si and Al. EELS spectra of the high-V areas resemble those of our V-oxide standards, confirming the presence of a nanoscale V-oxide phase within the illites, termed the V edge phase. In V-chlorite samples the V edge phase is absent. When leached, V-illites have a significantly higher V recovery than V-chlorites, suggesting that the higher V recovery in V-illites is caused by leaching of the nanometer V edge phase. Contrary to most current assumptions, the actual oxidation state of crystallographic V is mixed, with chlorites averaging 63% V^{3+} compared to a more oxidized 16% V^{3+} for the illites. It is unclear if the difference in V valence has an impact on the leachability of V, but for both chlorites and illites lacking the V edge phase, recoveries

were low. Overall, it is safe to conclude that the current metallurgical practice of assigning a single value for metal extraction, or gangue acid consumption, of phyllosilicates is overly simplistic. Actual acid consumption and metal extraction will vary depending on nanoscopic parameters such as the prevalence of metal and metal oxide phases, their solubility, their location at grain centers or edges, and likely the coordination and valence state of the crystallographic fraction of the metals. Further work is required to fully understand the prevalence of microscopic metal oxides within phyllosilicate minerals and the role of metal valence state in determining leachability.

8.0 References

Ahn, J. H., Xu, H., and Buseck, P.R., 1997, Transmission electron microscopy of native copper inclusions in illite: Clays and Clay Minerals, v. 45, p. 295-297.

Baker, C.E., and Sparling, D.K., 1981, Design and development of the White Mesa uranium mill, Mining Engineering, v. 33, p. 382-385

Barton, M.D., Barton, I.F., and Thorson, J.P., 2018a, Paleofluid flow in the Paradox Basin: Introduction, *in* Thorson, J.P., Paradox Basin fluids and Colorado Plateau copper, uranium and vanadium deposits field trip, Society of Economic Geologists, Guidebook Series, v. 59, p. 1-12

Barton, I.F., Barton, M.D., and Thorson, J.P., 2018b, Characteristics of Cu and U-V deposits in the Paradox Basin (Colorado Plateau) and associated alteration, *in* Thorson, J.P., Paradox Basin fluids and Colorado Plateau copper, uranium and vanadium deposits field trip, Society of Economic Geologists, Guidebook Series, v. 59, p. 73-102

Baum, W., 1999, The use of a mineralogical data base for production forecasting and troubleshooting in copper leach operations: Proceedings of the Copper 99 International Conference, Phoenix, Arizona, 1999.

Bickmore, B.R., Bosbach, D., Hochella, M.F., Charlet, L., and Rufe, E., 2001; In situ atomic force microscopy study of hectorite and nontronite dissolution: Implications for phyllosilicate edge surface structures and dissolution mechanisms: American Mineralogist, v. 86, p. 411-423.

Brandt, F., Bosbach, D., Krawczyk-Bärsch, E., Arnold, T., and Bernhard, G., 2002, Chlorite dissolution in the acid pH-range: A combined microscopic and macroscopic approach: Geochimica et Cosmochimica Acta, v. 67, p. 1451-1461.

Bos-Orent, E., 2021, Characterization of U(-V) deposits in the La Sal district, UT and CO and their relationship to Paradox Basin fluid flow, Masters Thesis, University of Arizona, Tucson, Arizona, retrieved from repository.arizona.edu.

Brigatti, M.F., Caprilli, E., Marchesini, M., and Poppi, L., 2003, The crystal structure of roscoelite-1M: Clays and Clay Minerals, v. 51, 301-308.

Brindley, G.W., and Youell, R.F., 1951, A chemical determination of ‘tetrahedral’ and ‘octahedral’ aluminium ions in a silicate: Acta Crystallographica, v. 4 p. 496-496.

Chetty, D., 2018, Acid-gangue interactions in heap leach operations: a review of the role of mineralogy for predicting ore behavior: Minerals, v. 8.

Foster, M.D., 1959, Chemical study of the mineralized clays, in Garrels, R.M. and Larsen, E.S., Geochemistry and mineralogy of the Colorado Plateau uranium ores, U.S. Geological Survey Professional Paper 302, p. 121-132.

Gao, F., Olayiwola, A.U., Liu, B., Wang, S., Du, H., Li, J., Wang, X., Cheng, D., and Zhang, Y., 2021, Review of vanadium production part I: primary resources: Mineral Processing and Extractive Metallurgy Review, v. 43, p. 466-488.

Gupta, C.K., 1985, Extractive metallurgy of niobium, tantalum, and vanadium: International Metals Reviews, v. 29, p. 405-444.

Ilton E.S., and Verblen D.R., 1993, Origin and mode of copper enrichment in biotite from rocks associated with porphyry deposits: a transmission electron microscopy investigation: Economic Geology, v. 88, p. 885-900.

Jansen, M., and Taylor, A., 2003, Overview of gangue mineralogy issues in oxide copper heap leaching: Proceedings of the ALTA Conference, Perth, Australia, 2003, p. 19-24.

Kalinowski, B.E., and Schweda, P., 1996, Kinetics of muscovite, phlogopite, and biotite dissolution and alteration at pH 1-4, room temperature: Geochimica et Cosmochimica Acta, v. 60, p. 367-385.

Kear, G., Shah, A.A., Walsh, F.C., 2011, Development of the all-vanadium redox flow battery for energy storage: a review of technological, financial and poly aspects: International Journal of Energy Research, v. 36 pp. 1105-1120.

Kelley, K.D., Scott, C.T., Polyak, D.E., and Kimball, B.E., 2017, Vanadium, chap. U *of* Schulz, K.J., DeYoung, J.H., Jr., Seal, R.R., II, and Bradley, D.C., eds., Critical mineral resources of the United States—Economic and environmental geology and prospects for future supply: U.S. Geological Survey Professional Paper 1802, p. U1–U36.

Kociak, M., Stéphan, O., Walls, M.G, Tencé, M., and Colliex, C., Spatially resolved EELS: The spectrum-imaging technique and its applications, in Pennycook, S.J., and Nellist, D.P., eds., Scanning Transmission Electron Microscopy, 1st ed.: New York, Springer New York, p. 163-205.

Li, M., Wei, C., Fan, F., Li., C., Deng, Z., and Li., X., 2009, Extraction of vanadium from black shale using pressure acid leaching: Hydrometallurgy, v. 98 p. 308-313.

Meunier, J.D., 1994, The composition and origin of vanadium-rich clay minerals in Colorado-Plateau Jurassic Sandstones, Clays and Clay Minerals, Vol. 42, No. 4, p. 391-401.

Osthaus, B.B., 1953, Chemical determination of tetrahedral ions in nontronite and montmorillonite: Second National Conference on Clays and Clay Minerals, Pittsburgh, 1953, pp. 404-417.

Peacor, D.R., Coveney, R.M., and Zhao, G., 2000, Authigenic illite and organic matter: the principle hosts of vanadium in the Mecca Quarry Shale at Velpen, Indiana: Clays and Clay Minerals, v. 48, pp. 311-316.

Polyak, D., 2018, U.S. Geological Survey Yearbook Vanadium.

Polyak, D., 2021, Vanadium: U.S. Geological Survey, Mineral Commodity Summaries.

Pourbaix, M., 1975, Atlas of electrochemical equilibria in aqueous solutions: Houston, National Association of Corrosion Engineers, 643 p.

Radwany, M., 2021, Geometallurgical characterization of sandstone-hosted vanadium ore from the Colorado Plateau. Masters Thesis, University of Arizona, Tucson, Arizona, retrieved from repository.arizona.edu.

Ross, G. J., 1969, Acid dissolution of chlorites: release of magnesium, iron, and aluminum and mode of acid attack: Clays and Clay Minerals, v. 17, p. 347-354.

Rozalen, M., Huertas, F.M., Brady, P.V., 2009, Experimental study of the effect of pH and temperature on the kinetics of montmorillonite dissolution: Geochimica et Cosmochimica Acta, v. 73, p. 3752-3766.

Slick, L.R., Chang, J.Y., and Zega, T., 2019, Calculation of chemical shift for Ti via EELS white-line-ratio method: Microscopy Microanalysis, v. 25, p. 662-663.

Snäll, S., and Liljefors, T., 2000, Leachability of major elements from minerals in strong acids: Journal of Geochemical Exploration, v. 71 p. 1-12.

Tan, H., Verbeeck, Jo., Abakumov, A., and Tendeloo, V.G., 2012, Oxidation state and chemical shift investigation in transition metal oxides by EELS: Ultramicroscopy, v. 116, p. 24-33.

Tavakoli, M.R., Dornian, S., and Dreisinger, D.B., 2014, The leaching of vanadium pentoxide using sulfuric acid and sulfite as a reducing agent, Hydrometallurgy, v. 141, p. 59-66.

Thorson, 2018, Paradox basin fluids and Colorado Plateau copper, uranium and vanadium deposits: overview, *in* Thorson, J.P., Paradox Basin fluids and Colorado Plateau copper, uranium and vanadium deposits field trip, Society of Economic Geologists, Guidebook Series, v. 59, p. 13-46.

Terry, B., 1983a, The acid decomposition of silicate minerals part II. hydrometallurgical applications: Hydrometallurgy, v. 10, p. 151-171.

Terry, B., 1983b, The acid decomposition of silicate minerals part I. Reactivities and modes of dissolution of silicates: Hydrometallurgy, v. 10, p. 135-150.

Wanty, R.B., and Goldhaber M.B., 1984, A method for the determination of vanadium and iron oxidation states in naturally occurring oxides and silicates: Talanta, v. 32, pp. 395-398.

Zhang, Y.M., Bao, S.X., Liu, T., Chen, T.J., and Huang, J., 2011, The technology of extracting vanadium from stone coal in China: history, current status and future prospects: Hydrometallurgy, v. 109, p. 116-124.

Zheng, Q., Zhang, T., Lieu, T., Huang, J., and Xue, N., 2019b, Vanadium extraction from black shale: Enhanced leaching due to fluoride addition: Hydromatlluergy, v. 187, p. 141-148.

Zheng, Q., Zhang, Y., Xue, N., Liu, T., and Huang, J., 2019a, Vanadium occupation and its leachability differences in trioctahedral and dioctahedral mica: RSC Advances, v. 9, p. 27615-27624.